RSC Advances

PAPER

View Article Online
View Journal | View Issue

Cite this: *RSC Adv.*, 2024, **14**, 160

Preparation of novel S-allyl cysteine chitosan based nanoparticles for use in ischemic brain treatment†

Mohd Faiyaz Khan,†[a] Niyaz Ahmad, †*[bc] Faisal K. Alkholifi,[d] Zabih Ullah,[e] Mohammed Saifuddin Khalid,[f] Sultan Akhtar, [g] Sadaf Farooqui,[a] Nazia Khan,[h] Anis Ahmad Chaudhary,[i] Abdullah S. Alawam[i] and Mohamed A. M. Ali[ij]

Objective: To enhance the brain bioavailability of *S*-allyl-L-cysteine (SC) by developing novel *S*-allyl-L-cysteine chitosan nanoparticles (SC CS NPs) and examining the quantity of SC by developing a novel method of ultra-high performance liquid chromatography-tandem mass spectrometry (UHPLC-MS/MS) in ischemic rat brain treatment. *Methods*: The ionotropic gelation method was used to develop *S*-allyl cysteine-loaded CS NPs. The 4-factor, 5-level central composite design was optimized to determine the effect of independent variables, *i.e.*, particle size, polydispersity index (PDI), zeta potential, EE, and loading capacity, together with their characterization, followed by drug release and intranasal permeation to enhance the brain bioavailability and examination of their neurobehavioral and biochemical parameters with their histopathological examination. *Results*: SC CS NPs were optimized at the particle size of 93.21 ± 3.31 nm (PDI: 0.317 ± 0.003), zeta potential of 44.4 ± 2.93, and drug loading of 41.23 ± 1.97% with an entrapment efficiency of 82.61 ± 4.93% having sustain and controlled release (79.92 ± 3.86%) with great permeation (>80.0%) of SC. SC showed the retention time of 1.021 min and 162.50/73.05 *m*/*z*. SC showed good linearity in the range of 5.0–1300.0 ng mL^{-1}, % inter-and-intraday accuracy of 96.00–99.06% and CV of 4.38–4.38%. We observed significant results, *i.e.*, $p < 0.001$ for improved $(AUC)_{0-24}$ and C_{max} delivered *via* i.v. and i.n. dose. We also observed the highly significantly observations of SC CS NPs (i.n.) based on their treatment results for the biochemical, neurobehavioral, and histopathological examination in the developed ischemic MCAO brain rat model. *Conclusion*: The excellent significant role of mucoadhesive CS NPs of SC was proven based on the enhancement in the brain bioavailability of SC *via* i.n. delivery in rats and easy targeting of the brain for ischemic brain treatment followed by an improvement in neuroprotection based on a very small dose of SC.

Received 31st August 2023
Accepted 13th November 2023

DOI: 10.1039/d3ra05933b

rsc.li/rsc-advances

Introduction

Presently, stroke has emerged as a significant global public health concern, leading to disabilities, and in severe cases, even fatalities. Ischemic stroke, resulting from any interruption in blood flow to the brain, initiates a cascade of events, including energy failure, triggering a series of intricate metabolic processes and culminating in neuronal cell death. This cascade of events leads to mitochondrial dysfunction, a rapid decline in adenosine triphosphate (ATP) levels, and subsequently the generation of free radicals and lipid peroxidation (LPO).[1,2]

[a]*Department of Clinical Pharmacy, College of Pharmacy, Prince Sattam Bin Abdulaziz University, Alkharj, Saudi Arabia*

[b]*Department of Pharmaceutics, College of Clinical Pharmacy, Imam Abdulrahman Bin Faisal University, P. O. Box 1982, Dammam, 31441, Kingdom of Saudi Arabia. E-mail: niyazpharma@gmail.com; Fax: +966 13 333 0290; Tel: +966 13 333 5541; +966 531203626*

[c]*Department of Pharmaceutical Sciences, Green Research Lab, Riyadh, Saudi Arabia*

[d]*Department of Pharmacology, College of Pharmacy, Prince Sattam Bin Abdulaziz University, Al Kharj, Saudi Arabia*

[e]*Department of Pharmaceutical Sciences, College of Pharmacy and Dentistry, Buraydah Colleges, Alqassim, Saudi Arabia*

[f]*Department of Pharmacology, College of Clinical Pharmacy, Imam Abdulrahman Bin Faisal University, Dammam, Kingdom of Saudi Arabia*

[g]*Department of Physics, Institute for Research and Medical Consultation (IRMC), Imam Abdulrahman Bin Faisal University, P. O. Box 1982, Dammam 31441, Saudi Arabia*

[h]*Department of Pharmaceutical Sciences, Ibn Sina National College for Medical Studies, Jeddah, Saudi Arabia*

[i]*Department of Biology, College of Science, Imam Mohammad Ibn Saud Islamic University (IMSIU), Riyadh, Saudi Arabia*

[j]*Department of Biochemistry, Faculty of Science, Ain Shams University, Abbassia, 11566, Cairo, Egypt*

† Co-first authors: Mohd Faiyaz Khan and Niyaz Ahmad – these authors contributed equally.

Oxidative stress and free radicals play a significant role in various models of acute and chronic cerebral injuries, as seen in neurodegenerative conditions and focal ischemic stroke.[3–5] Oxidative stress leads to cerebral injury due to the rapid oxidative metabolic activity, limited antioxidant capacity, higher concentration of polyunsaturated fatty acids, and inadequate neuronal cell repair mechanisms. Tissue damage occurs as a result of elevated levels of reactive oxygen species following cerebral ischemia, ultimately necessitating increased antioxidant intake and the deactivation of antioxidant enzymes. This means that the endogenous antioxidant defense mechanisms are insufficient to shield neurons from oxidative damage.[4–6] The brain tissue is particularly vulnerable to oxidative damage, highlighting the importance of pharmacological approaches to mitigate oxidative harm as a prominent avenue for stroke treatment.

Experimental models of cerebral ischemia have been established to expand our understanding of the mechanisms involved in cerebral ischemic injuries. These models also serve to evaluate the effectiveness of therapeutic or preventative strategies. Currently, one of the most widely used models for inducing focal brain ischemia is MCAO, which stands for middle cerebral artery occlusion. It is considered more reliable than all other reported animal models of ischemic stroke.[1,2,7] These models play a crucial role in the preclinical assessment of drugs aimed at protecting the brain, potentially leading to improved functional recovery following a stroke.

Further research is necessary to unravel the molecular intricacies underlying cerebral ischemic injuries. Oxidative stress stands out as a pivotal component in comprehending this mechanism and its potential treatments. Inflammation and excitotoxicity are additional distinguishing factors that contribute to the signaling pathways responsible for cell death in cases of cerebral ischemic stroke. This presents a significant opportunity to introduce novel clinical therapies for brain protection, with high efficacy and clinical priority.

S-allyl cysteine (SC) has been reported to possess anti-inflammatory and antioxidant properties. SC is the most active organosulfur compound found in garlic extracts.[5,8,9] This compound shows various therapeutic effects, particularly in relation to brain diseases such as Alzheimer's disease,[10] stroke,[11,12] and Parkinson's disease.[13] The molecular mechanisms underlying these effects include the protection of neurons against mitochondrial damage, oxidative stress, and subsequent cell death. SC has also been observed to reduce brain edema induced by ischemia in rats by inhibiting lipid peroxidation (LPO).[14] Additionally, *S*-allyl cysteine has demonstrated protective effects on neurons exposed to amyloid-β-peptide-induced oxidative damage and associated cognitive deficits.[15] Some research groups have also shown the neuroprotective effects of *S*-allyl cysteine in a middle cerebral artery occlusion (MCAO) model using male Wistar rats for the treatment of ischemic brain conditions.[5,16,17] However, it is important to note that *S*-allyl cysteine is water-soluble and has difficulty crossing the blood–brain barrier, resulting in low bioavailability in the brain. Therefore, it is necessary to enhance its bioavailability in the brain. In our research, we aimed to develop a nanometer-sized formulation to improve the brain bioavailability of *S*-allyl cysteine.

In recent times, researchers have become increasingly interested in intranasal drug delivery due to the advantages offered by nanoparticles. These advantages include bypassing the hepatic first-pass metabolism, overcoming the blood–brain barrier, and providing a convenient, non-invasive route for drug administration.[2,18,19] However, it is crucial to consider that drugs delivered intranasally tend to have a short residence time in the nasal passage. Therefore, a key parameter in developing novel nanoformulations for intranasal use is to enhance their mucoadhesion and viscosity, which extends the residence time of drugs in the nasal passage. Mucoadhesive nanoformulations for intranasal delivery can lead to increased drug absorption. In this context, there is a need for novel formulations that enhance the nasal staying time, particularly focusing on mucoadhesive properties. Accordingly, *S*-allyl cysteine can be encapsulated in biodegradable and biocompatible nanoparticles, such as *in situ* nasal gel nanoformulations. This approach offers an alternative method for intranasal drug delivery.[20–22] These nanoparticles play a crucial role in improving the therapeutic effects, controlling the drug release, achieving the maximum drug loading, and increasing the surface area of drugs. Polymeric nanoparticles, with their unique properties, allow for rapid drug release and targeted delivery to specific tissues and organs, including the brain. Furthermore, they offer the advantage of protecting the drugs by encapsulating them in the formulation core, reducing extracellular or chemical delivery through P-glycoprotein efflux. This approach has shown improved bioavailability in the brain and benefits conditions such as ischemic brain, epilepsy, and Parkinson's disease *via* the olfactory membranes.[2,20–22] Therefore, this nanoformulation represents a novel approach compared to other intranasal delivery methods. Chitosan, a polysaccharide composed of *N*-acetyl-D-glucosamine and glucosamine linked by β-(1–4) glycosidic bonds, is a commonly used polymer with mucoadhesive properties.[23] It has various beneficial biological properties, including mucoadhesion, enhanced penetration, non-immunogenicity, antibacterial qualities, non-carcinogenicity, non-toxicity, and biocompatibility, for intranasal drug delivery and blood–brain barrier traversal. Furthermore, the mucoadhesive nature of chitosan increases the nasal residence time, enhancing the drug permeation to the nasal mucosa and increasing the bioavailability of the drug.[1,21,22] Alternatively, the surface modification of chitosan nanoparticles offer several advantages, as follows: (i) controlled and sustained drug release, combined with mucoadhesive drug delivery systems; (ii) improved drug absorption and extended drug release; (iii) reduction of burst drug release through chitosan coating; (iv) enhanced drug permeation; and (v) increased retention of nanoparticles due to the interactions between the positively charged chitosan and negatively charged membranes.[1,20–22,24,25,31,45–48]

The aim of this study was to apply this approach to develop a nanoformulation using chitosan (CS) as the base, with the primary objective of enhancing the bioavailability of *S*-allyl cysteine (SC) in the brain through intranasal delivery of SC-loaded CS nanoparticles (SC CS NPs). Our research focused on achieving the maximum SC concentration in the brain, while

minimizing systemic exposure and using the lowest therapeutic dosage required. Carrier systems such as CS NPs have demonstrated increased permeability and solubility. Accordingly, *S*-allyl cysteine-loaded nanoparticles were formulated and assessed for various physicochemical characteristics, specifically to evaluate their ability for nose-to-brain delivery of SC. Novel nanoparticles for SC were developed and a comparative analysis of the bioavailability of *S*-allyl cysteine (SC) and the pharmacokinetic parameters (including AUC_{0-t}, $t_{1/2}$, C_{max}, and K_{el}) between SC-S and SC-NPs in the brain was conducted. It is worth noting that there is currently no established bioanalytical method for determining or analyzing the bioavailability of *S*-allyl cysteine in the brain or its homogenate in the literature.[26–29] Thus, there is a need to develop novel bioanalytical methods capable of quantifying *S*-allyl cysteine at nanogram levels.

The primary objective of our research was to thoroughly investigate the optimization of *S*-allyl cysteine-loaded chitosan nanoparticles (SC CS NPs), with a focus on assessing their mucoadhesive properties, *in vitro* release characteristics, and ability to permeate the nasal mucosa. We employed a novel method using UHPLC MS/MS to quantify *S*-allyl cysteine in the brain and plasma at nanogram levels for the first time. The critical aspect of our investigation involved evaluating the potential of SC CS NPs for ischemic brain treatment and comparing their pharmacokinetic parameters, together with an assessment of their neuroprotective effects. The bioavailability of *S*-allyl cysteine was enhanced successfully in the brain *via* intranasal administration, while minimizing side effects. Our work represents a pioneering effort in the literature, given that we developed novel nanoparticles with mucoadhesive properties for the delivery of *S*-allyl cysteine. Furthermore, we applied the *S*-allyl cysteine CS NPs for the first time in ischemic brain treatment and conducted thorough ex vivo and *in vitro* assessments.

Materials and methods

S-allyl-L-cysteine and chitosan were purchased from Sigma, USA. Chitosan (molecular weight: 50 000–190 000 Da and degree of deacetylation: 75–85%) was purchased from Sigma-Aldrich Chemicals Co., St. Louis, MO, USA. LC-MS-grade solvents including ammonium formate, acetonitrile, ammonium acetate, methanol, formic acid were purchased from Sigma-Aldrich Corporation, USA and other chemicals were analytical grade. All experiments were performed using Milli Q water.

Preparation of CS nanoparticles

The ionotropic gelation technique was applied for the formulation of the CS NPs.[1,30] We prepared an acetic acid aqueous solution (1.0%) to dissolve and prepare different concentrations of chitosan. Milli Q water was used to dissolve TPP (tripolyphosphate: cross linking agent). SC was dissolved in the CS-solution during the preparation of the nanoparticles. The CS solution with SC was added to a beaker and stirred with a magnetic stirrer (different rpm, *i.e.*, 600 to 1000) at room temperature and the TPP solution slowly added. A suspension (opalescent form) was formed and left for thirty minutes for more crosslinking to optimize the SC CS NPs. After the optimization, the SC CS NPs were centrifuged (18 000 rpm at 4.0 °C), and after that freeze-dried in a lyophilizer (Lab Conco., USA) for one day at 100.0 mbar and −120.0 °C with the help of 1.0% mannitol as a cryoprotectant. According to the prepared formulations, central composite design (CCD; Stat-Ease Inc., USA) was applied, *i.e.*, the to optimize the NPs.

Application of CCD design

CCD (4-factor and 5-level) was applied to optimize the relation between the dependent and independent variables of concentration of tripolyphosphate and CS, pH and stirring speed, and ZP, PDI, PS, %DL, and %EE (Table 1).[31] We have formulated a thirty run trial-based CCD design (Table 2).

CCD explored the quadratic response surfaces based on the following polynomial equation:

$$Y = b_0 + b_1X_1 + b_2X_2 + b_3X_3 + b_4X_4 + b_{12}X_1X_2 + b_{14}X_1X_4 + b_{23}X_2X_3 + b_{24}X_2X_4 + b_{34}X_3X_4 + b_{11}X_{12} + b_{22}X_{22} + b_{33}X_{32} + b_{44}X_{42} \quad (1)$$

where Y_1 is the particle size, Y_2 is the polydispersity index, Y_3 is the zeta potential, Y_4 is the loading capacity, and Y_5 is the entrapment efficiency chosen according to the dependent variables based on some limits for Y_1 (≤100.0 nm) and Y_2 (≤50.0 mV) that is necessary for brain targeting *via* intranasal

Table 1 Variables in "Design Expert" software for the preparation and optimization of *S*-allyl cysteine-chitosan-nanoparticles (SC-NPs)

Factors	Levels		
Independent variables	**Low level (−1)**	**Level (0)**	**High level (+1)**
X_1 = chitosan (%)	0.05	0.15	0.25
X_2 = TPP (%)	0.05	0.15	0.25
X_3 = speed (rpm)	600	800	1000
X_4 = pH	4.0	5.0	6.0
Dependent variables	**Constraints**		
Y_1 = particle size (PS: nm)	Minimize		
Y_2 = polydispersity index (PDI)	Minimize		
Y_3 = zeta potential (ZP: mV)	Maximize		
Y_4 = loading capacity (DL: %)	Maximize		
Y_5 = entrapment efficiency (EE: %)	Maximize		

Table 2 *S*-Allyl cysteine (SC)-nanoparticles suggested through "Design Expert" software including 13 independent variables and their responses

	Independent variables				Dependent variables									
	Coded factors				Observed (actual) responses					Predicted responses				
Formulation code	X_1	X_2	X_3	X_4	Y_1	Y_2	Y_3	Y_4	Y_5	Y_1	Y_2	Y_3	Y_4	Y_5
SC-NPs 1	0.05	0.05	600	4	298.28 ± 25.01	0.583 ± 0.005	30.1 ± 2.01	34.56 ± 2.16	62.85 ± 4.09	298.86	0.588	30.04	33.98	62.78
SC-NPs 2	0.25	0.05	600	4	201.17 ± 18.03	0.477 ± 0.004	27.7 ± 1.64	35.64 ± 2.07	64.25 ± 4.11	201.75	0.476	27.63	35.82	64.18
SC-NPs 3	0.05	0.25	600	4	286.82 ± 22.84	0.564 ± 0.005	23.3 ± 1.48	36.53 ± 2.00	66.89 ± 3.64	287.32	0.569	23.28	36.71	66.84
SC-NPs 4	0.25	0.25	600	4	249.53 ± 20.11	0.459 ± 0.003	24.8 ± 3.79	39.76 ± 1.98	72.43 ± 5.09	250.03	0.457	24.75	39.65	72.37
SC-NPs 5	0.05	0.05	1000	4	218.18 ± 18.93	0.609 ± 0.005	34.4 ± 5.08	31.81 ± 3.14	70.19 ± 4.85	218.61	0.615	34.34	31.99	70.14
SC-NPs 6	0.25	0.05	1000	4	174.28 ± 17.21	0.504 ± 0.003	27.2 ± 4.18	33.39 ± 2.16	58.80 ± 3.94	174.71	0.502	27.15	33.28	58.75
SC-NPs 7	0.05	0.25	1000	4	283.14 ± 21.08	0.591 ± 0.007	28.8 ± 3.78	37.45 ± 2.64	68.46 ± 4.82	286.88	0.596	28.78	37.34	68.43
SC-NPs 8	0.25	0.25	1000	4	302.57 ± 25.31	0.485 ± 0.004	25.5 ± 4.00	39.79 ± 2.66	61.21 ± 4.29	302.81	0.484	25.46	39.74	61.18
SC-NPs 9	0.05	0.05	600	6	318.63 ± 27.08	0.608 ± 0.008	27.6 ± 3.15	38.92 ± 1.98	60.34 ± 3.77	318.34	0.612	27.66	39.07	60.37
SC-NPs 10	0.25	0.05	600	6	195.53 ± 18.41	0.502 ± 0.006	29.7 ± 2.84	39.26 ± 2.01	66.37 ± 4.08	195.24	0.499	29.72	39.13	66.41
SC-NPs 11	0.05	0.25	600	6	244.59 ± 20.02	0.590 ± 0.007	23.2 ± 3.66	43.04 ± 1.67	61.59 ± 3.43	243.99	0.594	23.26	42.91	61.66
SC-NPs 12	0.25	0.25	600	6	181.32 ± 18.11	0.484 ± 0.005	29.1 ± 2.47	44.14 ± 3.18	71.76 ± 3.61	180.72	0.482	29.19	44.07	71.83
SC-NPs 13	0.05	0.05	1000	6	203.96 ± 19.04	0.634 ± 0.006	29.9 ± 3.31	36.67 ± 2.96	77.08 ± 3.94	203.18	0.639	29.98	36.54	77.17
SC-NPs 14	0.25	0.05	1000	6	134.08 ± 12.04	0.529 ± 0.004	27.2 ± 3.14	36.12 ± 2.51	70.33 ± 4.18	133.3	0.526	27.26	36.05	70.42
SC-NPs 15	0.05	0.25	1000	6	209.84 ± 10.35	0.616 ± 0.007	26.6 ± 2.31	43.08 ± 3.38	72.55 ± 4.61	208.64	0.620	26.76	43.01	72.69
SC-NPs 16	0.25	0.25	1000	6	199.79 ± 14.21	0.511 ± 0.004	27.8 ± 2.64	43.28 ± 4.01	69.94 ± 3.34	198.59	0.508	27.93	43.62	70.08
SC-NPs 17	0.15	0.16	830	5.3	93.21 ± 3.31	0.317 ± 0.003	44.4 ± 2.93	41.23 ± 1.97	82.61 ± 4.93	99.24	0.351	40.98	41.14	79.21
SC-NPs 18	0.35	0.15	800	5	126.8 ± 10.27	0.441 ± 0.003	20.4 ± 1.31	39.46 ± 1.83	66.00 ± 4.16	127.08	0.452	20.39	39.41	65.97
SC-NPs 19	0.15	0.05	800	5	302.82 ± 20.11	0.565 ± 0.004	31.9 ± 2.83	33.25 ± 1.64	56.29 ± 3.00	303.31	0.562	31.86	33.44	56.24
SC-NPs 20	0.15	0.35	800	5	357.07 ± 22.73	0.528 ± 0.004	25.8 ± 1.67	43.78 ± 3.37	59.95 ± 3.49	357.06	0.526	25.77	43.73	59.95
SC-NPs 21	0.16	0.15	800	5.5	147.34 ± 13.06	0.450 ± 0.005	29.0 ± 1.57	39.62 ± 2.95	67.22 ± 3.91	148.91	0.423	28.91	39.81	67.15
SC-NPs 22	0.15	0.15	800	5	165.71 ± 13.02	0.473 ± 0.006	31.9 ± 2.79	37.41 ± 1.32	72.74 ± 5.46	167.53	0.431	31.94	37.36	72.76
SC-NPs 23	0.15	0.15	800	3	240.66 ± 13.94	0.521 ± 0.004	30.5 ± 3.18	33.24 ± 2.11	70.95 ± 5.09	240.54	0.516	30.5	33.38	70.96
SC-NPs 24	0.05	0.15	800	5	233.96 ± 12.46	0.693 ± 0.006	21.7 ± 1.54	36.77 ± 1.67	67.21 ± 3.11	234.24	0.677	21.64	36.96	67.18
Centre points														
SC-NPs 25	0.15	0.15	800	5	133.44 ± 11.94	0.547 ± 0.004	40.8 ± 2.47	40.34 ± 1.86	78.00 ± 5.39	128.59	0.547	41.35	40.36	78.55
SC-NPs 26	0.15	0.15	800	5	133.44 ± 11.94	0.547 ± 0.004	40.8 ± 2.47	40.34 ± 1.86	78.00 ± 5.39	128.59	0.547	41.35	40.36	78.55
SC-NPs 27	0.15	0.15	800	5	133.44 ± 11.94	0.547 ± 0.004	40.8 ± 2.47	40.34 ± 1.86	78.00 ± 5.39	128.59	0.547	41.35	40.36	78.55
SC-NPs 28	0.15	0.15	800	5	133.44 ± 11.94	0.547 ± 0.004	40.8 ± 2.47	40.34 ± 1.86	78.00 ± 5.39	128.59	0.547	41.35	40.36	78.55
SC-NPs 29	0.15	0.15	800	5	133.44 ± 11.94	0.547 ± 0.004	40.8 ± 2.47	40.34 ± 1.86	78.00 ± 5.39	128.59	0.547	41.35	40.36	78.55
SC-NPs 30	0.15	0.15	800	5	133.44 ± 11.94	0.547 ± 0.004	40.8 ± 2.47	40.34 ± 1.86	78.00 ± 5.39	128.59	0.547	41.35	40.36	78.55

permeation of the drug, followed by maximum stability duration. All the variables for CS–NPs are listed in Table 2.

CCD data analysis by statistics

ANOVA was applied for the analysis of all runs followed by their statical validation based on integrated software. The results showed appropriate quadratic, 2Fl, cubic, and linear models, which were employed to analyze the statistics of coefficients. The Design Expert® software was applied based on the probability and lattice to determine the concentration or ration of various components for the prepared nanoparticles. All the variables were plotted three-dimensionally using the Design Expert® software. Various checkpoints were examined to evaluate the characteristics of their different responses. The % prediction error was examined with the help of the result comparison determined through data and observation results from software.

Examination of particle size, ZP, and PDI

We assessed the particle size, zeta potential (ZP), and polydispersity index (PDI) to determine the surface area available for drug absorption. These measurements were carried out using a Zetasizer based on dynamic light scattering (Malvern Zetasizer, UK). The formulation was appropriately diluted prior to the particle size analysis, which was performed at 25 °C with a fixed scattering angle. Each sample was analyzed three times after diluting the prepared nanoparticles to assess their particle size.[1]

Characterization by TEM analysis

Transmission electron microscopy (TEM) was used to examine the size, shape, and structure of the NPs. The sample was added in dispersed form to a grid containing holes of a carbon support film. We left the grids with the sample to air-dry, and subsequently their TEM recorded.

We analysed the size of the samples using their images.[1]

Analysis of process yield, EE, and LC for optimized formulation

All samples were centrifuged up to 18 000 rpm for 40 min at a temperature of 4 °C for the evaluation of the LC and EE of the prepared NPs. The quantity of freely available *S*-allyl cysteine

was examined using our developed method and the supernatant of the sample. All preparations were evaluated three times for EE and LC according to the following equations:[31]

$$\text{EE } (\%) = \frac{\text{whole quantity of SC} - \text{freely available SC quantity}}{\text{whole quantity of SC}} \quad (2)$$

$$\text{LC } (\%) = \frac{\text{whole quantity of SC} - \text{freely available SC quantity}}{\text{mass of NPs}} \quad (3)$$

The following formula was applied for the process yield (%) calculation:

$$\text{Process yield } (\%) = \frac{\text{dry weight of nanoparticles } (W_1)}{\text{dry basis of whole mass of initial NPs } (W_2)} \quad (4)$$

Stability study

Initially, the SC CS NPs were dried by freeze-drying, and then dispersed in phosphate buffer saline (PBS, pH: 7.40). The SC CS NPs were stored at 4.0 °C for six months in the dark. Analysis was started at 0.0, and after 1.0 3.0, and 6.0 months to examine the EE (%), PDI, particle size, and ZP.[31] The *S*-allyl cysteine solution and SC CS NPs were tested as the test solution under 276 nm UV-light to examine their stability. The samples were diluted at intervals of 30 min, one hour, and two hours for the further quantitation of SC in both preparations.

S-Allyl cysteine release study

The *in vitro* release of *S*-allyl cysteine was examined using SC CS NPs kept in dialysis bags.[31] Phosphate buffer was prepared and kept pH 7.4 for the analysis of the release of SC from the SC CS NPs and the temperature was set at 37 °C for 6 h with stirring at a speed of 100 rpm by a stirrer. Initially, the dialysis bag was checked to ensure that there was no leakage, and then 0.5 mg SC added, *i.e.*, SC CS NPs. The release of SC from the SC CS NPs was evaluated at intervals of 30 min, 1 h, 2 h, 4 h, 6 h, 8 h, 10 h, 12 h, and 24 h by withdrawing 1 mL of sample. Each sample was filtered through a 0.2 μm syringe filter after its withdrawal and added to HPLC vials for analysis *via* LC-MS/MS, as reported in the literature.[1]

S-Allyl cysteine permeation *via* nasal passage

Fresh nasal mucosa was collected from goats at the Dammam slaughterhouse. A 0.785 cm^2 area of nasal mucosa was used for analyzing the permeation of SC using a Logan Instrument system from the USA. The receptor chamber contained 200 mL of phosphate buffer (pH 7.40) and was maintained at 37 °C. SC-loaded chitosan nanoparticles (SC CS NPs) were introduced in the donor chamber (21.5 mL) after preincubation at specific intervals. At each time point, 500 μL sample was collected from the receptor chamber, filtered through a 0.20 μm syringe filter, and transferred to HPLC vials for subsequent LC-MS analysis. The LC-MS methodology used was discussed in detail in ref. 31.

Animal study

Our research proposal was approved (IRB-2019-05-015) by the Imam Abdulrahman Bin Faisal University IRB Committee for the examination of both the PK and PD study parameters. Specifically, rats weighing 200–250 g were kept in a natural light and dark cycle. The rats were housed under the living conditions of 50% to 55% humidity and temperature of 20–30 °C and given free access to food and water. All animals were divided based on their groups in cages. The research was conducted only when the rats were moving freely while they were awake.

Development of LC-MS bioanalytical method and its validation for *S*-allyl-L-cysteine

An LCMS-8050 (ESI, triple quadrupole, Shimadzu) and C-18 column (100 mm, 1.7 μm, Waters) were used for the successful development of a bioanalytical method for SC, which has many advantages, *i.e.*, novel, highly sensitive (nanogram level), high resolution with great separation using a Shimadzu UHPLC, and very short run time (<2.0 min). The mobile phase was [CH_3OH : HCOOH (0.10%), 92 : 08], with a flow rate of 0.30 mL min^{-1}, injection volume of 10 μL, and very short run time of 2.0 min. Argon gas was used as the collision gas, the scan time was 1 min and the inter scan was 0.02 s with 30 000 μs and 0.10 μ scan steps. The +ve ion mode and collision energy (−13.0 eV) were used for the quantification of SC and the mass spectra are shown in Fig. 6. The quantity of SC in plasma was determined using the 5.93 Version Lab Solution Software (Kyoto, Japan). All samples (CC and QC) were freshly prepared, and unknown plasma samples were quantified (Fig. 7). The US-FDA guidelines were followed at the time of method validation, which gave excellent results based on the fitting relationship of concentration-detector response and regression equation ($1/x^2$).[31]

PK evaluation

All 4 groups were examined to determine the parameters of PK, which were divided as follows: group 1: SC S (i.n.), group 2: SC S (i.v.), group 3: SC CS NPs (i.n.), and group 4: SC CS NPs (intravenously) and the administered dose of SC was 15.0 mg per kilogram body wt. Four animals were taken at each sampling point from the four groups. Initially, the blood was withdrawn, and then the brain and lungs obtained rapidly by sacrificing them. All the samples were extracted first with the help of 750 μL different matrix samples (2.0% acetic acid in methanol + ethyl acetate), and then the different matrix samples analysed to examine all the parameters of PK. All the samples withdrawn based on the selected time points of pre-dose, 30 min, 1 h, 2 h, 4 h, 8 h, 12 h, and 24 h. PK parameters including AUC_{0-t}, elimination rate-constant, half-life, and C_{max} were analysed based on our developed LC-MS bioanalytical method. Each group consisted of 32 rats (4 in each point × 8-total-sampling time points) and 128 animals (32 × 4 = total 128 animals) were used for PK evaluation. We withdrew the blood first, and then the brain and lungs harvested rapidly by sacrificing 4 rats

at each point. After collection, the sample was homogenized, followed by extraction, and then transferred to vials for the determination of PK.[31]

Ischemic brain examination

A total of five groups was employed to examine the pharmacodynamic parameters *i.e.*, total of 30 rats ($5 \times 6 = 30$). All groups were treated separately, *i.e.*, SHAM: G-I, MCAO group: G-II, G-3: SHAM + CS NPs, *i.e.*, without SC means substantial control group, G-IV: MCAO + SC-S (15.0 mg per kg body wt; intranasally), and G-V: MCAO + SC CS NPs (15.0 mg per kg body wt; intranasally). The method reported by Longa *et al.* was used to develop ischemia in the rats for the MCAO model with the help of intraluminal filament insertion.[7] All studies were evaluated after 22 h of reperfusion including flexion (FT) tests, rotarod, spontaneous motor activity (SMA), and grip strength, where the rats were sacrificed serially to harvest their brain and lungs to perform the tests, followed by the histopathological study.

Neurobehavioral study

Rotarod study. Rotarod apparatus (Omnitech, USA) was employed to determine the coordination of the muscles in the rats after 22 h of reperfusion, as reported previously.[32] All rats were trained for 6 days to initiate our research study. We employed 4 animals at a time to perform the experiment, which had four sections on rotating rod (75 mm^2). We noted the time the rats fell from the rotating shaft *via* an omni-rotor. The cutoff time was 180 s at the rotating-shaft speed of 10 cpm. We determined the latency time or rotating rod time, which was previously fixed based on the staying time of each rat.

Examination of spontaneous motor activity (SMA). SMA was also examined based on the method reported by Ahmad *et al.*,[1] after 24 h of reperfusion. The animals were kept in their cages as described in groups for 5 min to evaluate the SMA. The scores for neurological assessment were considered as freely moving rats based on the free atmosphere independently = 0 and 1: hesitation to touch the walls of the cage but not touch; 2: there is an indication of postural defectiveness curved towards the paretic side due to not moving properly or very bad movement; and 3: no movements of the rats observed, which clearly indicating the postural defectiveness curved towards the paretic side.

Flexion test (FT). The method reported by Vaibhav *et al.*[33] was used to perform the FT test. Based on their scoring, the scaling was 0: there is no neurological deficit; 1: adduction of shoulder and wrist flexion, indicating contralateral forelimb flexion; 2: there is a decrement in lateral push resistance; and 3: there is movement inside the paretic side of the circle.

Grip strength examination. The method reported by Ahmad *et al.* was followed for the examination of grip strength.[2] The researchers tied a long string (50.0 cm) between two perpendicular supports and used the following scale to evaluate the grip strength: 0 (zero) = rat fell off; 1 (one) = hanging of rats continuously with 2 fore paws on the string; 2 (two): there is no difference but animals tried to climb on the string; 3 (three): animals hanged with both front paws on the string but one or both limbs were hind; 4 (four): tails were wrapped on the string and also hanged with the help of their two front paws; and 5 (five): the rats escaped.

Biochemical studies

Preparation of tissue. The brain was removed after sacrificing the rats, followed by cutting to remove the cortex area. All the brain tissues were homogenized [5% w/v] in PBS (10.0 mmol L^{-1}, 7.4 pH) and centrifuged (800 g for 5 min at 4.0 °C) to obtain the supernatant, which was denoted as S1. A very small quantity of S1 was employed to calculate the TBARS. If there was any remaining supernatant, then it was centrifuged (10 500*g*) again for 15 min at 4 °C. We also collected the supernatant again, *i.e.*, S2, and performed all the assay tests, *e.g.*, glutathione peroxidase (GPx), catalase (CAT), superoxide dismutase (SOD), and glutathione reductase (GR).

Examination of LPO. The TBARS assay was performed to examine LPO *via* its byproduct of lipid peroxidation using the method reported by Ahmad *et al.*[2] The sample homogenate (100 μL) was incubated at 37 °C in a metabolic water bath shaker. Then, 100 μL of the same homogenate was incubated at 0.0 °C. TCA (10%, 500 μL) and TBA TCA (0.67%, 500 μL) were transferred to both homogenate samples after incubation, and then both samples centrifuged again at 3000*g* for 15 min. The supernatant of both samples was collected and transferred to two fresh tubes, and then kept on a boiling water bath for 10 min. The tubes were left to cool to room temperature followed by the analysis of the samples at 535 nm. The results were calculated for the LPO rates in μmol of TBARS formed per h per g tissue using a molar extinction coefficient of 1.56×10^5 M^{-1} cm^{-1}.

Examination of glutathione peroxidase (GPx). GPx was determined based on the previously reported method by Mohandas *et al.*[34] and Ahmad *et al.*[2] All samples were mixed with PB (1.44 mL, 7.4 pH; 0.10 M), (0.10 mL, 1.0 mM) EDTA, Na-azide (0.1 mL 1 mM), GR (0.05 mL 1 U mL^{-1}), and reduced glutathione (0.05 mL, 1 mM). Then 10 μL of 0.25 mM hydrogen peroxide, PMS (100 μL, 10%), and 100 μL NADPH (0.2 mM) were transferred to a 2 mL volumetric flask and the volume made up to the mark. The disappearance of NADPH was measured at 340 nm at room temperature. The enzyme activity was calculated in μmol of NADPH oxidized per min per mg protein using the molar extinction coefficient of 6.22×10^3 M^{-1} cm^{-1}.

Determination of glutathione reductase (GR). GR was determined based on the previously reported method by Mohandas *et al.*[34] and Ahmad *et al.*[2] A mixture of 1.650 mL PB (0.10 M, 7.6 pH), PMS (10%, 100 μL), 0.1 M NADPH (100 μL), 50 μL GSSG (1 mM), and 100 μL of 0.5 mM EDTA was transferred to a 2 mL volumetric flask and the volume made up to the mark. The activity of the enzyme was determined based on the disappearance of the absorbance of NADPH at 340 nm. This was reported as nmol of NADPH oxidized per min per mg protein using the molar extinction coefficient of 6.22×10^3 M^{-1} cm^{-1}.

Determination of superoxide dismutase (SOD). The method reported by Ahmad *et al.* was used for the calculation of SOD activity.[2] A 1 mL mixture consisting of 100 μL PMS (10.0% w/v),

600 μL 0.50 M pH 7.4 PBS, 100 μL 57 mM NBT, and 100 μL 1 mM xanthine was incubated at 25 ± 5 °C for 15 min and 50 mU xanthine oxidase added to initiate the reaction. The changes in absorbance at 550 nm were monitored.

Determination of catalase (CAT). The method reported by Ahmad *et al.* was used for the calculation of catalase (CAT).[2] A 3 mL mixture was made containing of 50 μL of 10% PMS, 950 μL 0.019 M H_2O_2, 2 mL 0.1 M pH 7.4 PBF. The changes in absorbance at 240 nm were monitored to calculate CAT in nmol of H_2O_2 consumed per min per mg protein using the molar extinction coefficient of 40 M^{-1} cm^{-1}.

Determination of protein. The Bradford method was used to examine the quantity of protein[35] according to the method reported by Ahmad *et al.*[2] using bovine serum albumin as the standard.

Histopathological study

The brains of the rats were obtained from each group, and then placed in fresh phosphate buffer solution + 30% sucrose.[2] The cryostat technique (Leica, Nuβloch, Heidelberg, Germany) was used for the sectioning of 12 μm coronal sections of the brain in slice form. Glass slides were mounted for 10 cortex areas sections and eosin and hematoxylin used as the staining agent.

Applied statistics

The calculated data are reported as mean ± standard error of mean (SEM). ANOVA was applied using Student's *t*-test for the calculation of the mean values as two statistical unpaired examinations. The statistical significance of all the results was determined based on the *p*-value (<0.05).

Results and discussion

CCD-based optimization of CS NPs

CCD was used for the development and optimization of the *S*-allyl cysteine (SC) CS NPs. The results from the optimization of the *S*-allyl cysteine (SC) CS NPs were EE of 82.61 ± 4.93%, PS of 93.21 ± 3.31 nm, PDI of 0.317 ± 0.003, and ZP of +44.4 ± 2.93 mV, based on the compositions of their independent variables, *i.e.*, 0.15% [chitosan], 0.16% [TPP], 830 rpm [stirring speed], and 5.3 [pH].

The CCD software was used to characterize the surface of the NPs, giving ±1 and 0 for three levels. Furthermore, the CCD software was used for the appropriate design based on the statistics required in which the important parameter was the limited number of experiments required for a 4-factorial-level. The responses selected were dependent on the independent variable at the time of variable optimization and gave the results for a particular particle size, ZP, highest EE, PDI, and maximum LC. Based on the CCD results, the quadratic model was the best-fitted model for the values obtained for particle size, ZP, highest EE, but PDI and LC were linear. The best-fitting models for our suggested independent variables based on CCD are shown in Table 2. The independent variables were correlated with various coefficient value, *i.e.*, particle size, ZP, EE, PDI, and LC, which are dependent variables, and the obtained results were highly significant, as shown in Tables 3 and 4.

All the results were dependent on chitosan and TPP with speed (RPM) and their pH, as shown in Tables 1–4. Based on the observation, an increase in the concentration of CS and TPP (0.05% to 0.25%) also increased the particle size. The results showed a decrease or increase in sonication time ⟨830 rpm⟩ and pH ⟨5.3⟩, with a great increase in the particle size observed (Table 2).

Effect of independent variables on particle size

The average particle size was employed for all four independent variables (Fig. 1A). The concentration chitosan (0.15% w/v) and TPP (0.16%, w/v) was optimized at the stirring speed of 830, and solution pH of 5.3, and minimum particle size of 93.21 ± 3.31 nm. Finally, it was confirmed that the concentration of CS is directly proportional to the particle size. This can be due to

Table 3 Results of regression analysis for responses Y_1 = particle size (PS: nm), Y_2 = polydispersity index (PDI), Y_3 = zeta potential (ZP: mV), Y_4 = loading capacity (DL: %), and Y_5 = entrapment efficiency (EE: %)

Quadratic model	R^2	Adjusted R^2	Predicted R^2	Standard deviation (SD)	Coefficient of variation (CV) (%)
Response (Y_1)	0.9925	0.9855	0.9896	8.37	3.99
Response (Y_2)	0.9922	0.9849	0.9483	0.007	1.23
Response (Y_3)	0.9894	0.9794	0.9891	0.953	3.09
Response (Y_4)	0.9975	0.9951	0.9841	0.2334	0.60
Response (Y_5)	0.9904	0.9815	0.9866	0.9487	1.36

$Y_1 = +128.59 - 26.79125 \times X_1 + 13.44 \times X_2 - 15.60 \times X_3 - 21.19 \times X_4 + 14.96 \times X_1X_2 + 13.3 \times X_1X_3 - 6.50 \times X_1X_4 + 19.96 \times X_2X_3 - 15.70 \times X_2X_4 - 8.73 \times X_3X_4 + 13.02 \times X_1^2 + 50.40 \times X_2^2 + 22.03 \times X_3^2 + 17.40 \times X_4^2$ (eqn (1))

$Y_2 = +0.547 - 0.056175 \times X_1 - 0.0091 \times X_2 + 0.013 \times X_3 + 0.012 \times X_4 + 0.0 \times X_1X_2 + 0.0 \times X_1X_3 + 0.0 \times X_1X_4 + 3.27 + 0.0 \times X_2X_36.54 \times X_2X_4 + 9.81 + 0.0 \times X_3X_4 + 0.004 \times X_1^2 - 0.0 \times X_2^2 - 0.0 \times X_3^2C^2 - 0.0 \times X_4^2$ (eqn (2))

$Y_3 = +41.35 - 0.3125 \times X_1 - 1.53 \times X_20.7589 \times X_3 + 0.02 \times X_4 + 0.97 \times X_1X_2 - 1.19 \times X_1X_3 + 1.12 \times X_1X_4 + 0.29 \times X_2X_3 + 0.59 \times X_2X_4 - 0.5 \times X_3X_4 - 5.08 \times X_1^2 - 3.13 \times X_2^2 - 2.73 \times X_3^2 - 2.70 \times X_4^2$ (eqn (3))

$Y_4 = +40.36 + 0.62 \times X_1 + 2.57 \times X_2 - 0.61 \times X_3 + 2.24 \times X_4 + 0.25 \times X_1X_2 - 0.14 \times X_1X_3 - 0.45 \times X_1X_4 + 0.66 \times X_2X_3 + 0.278 \times X_2X_4 - 0.14 \times X_3X_4 - 0.5426 \times X_1^2 - 0.44 \times X_2^2 - 0.44 \times X_3^2 - 0.63 \times X_4^2$ (eqn (4))

$Y_5 = +78.55 - 0.303 \times X_1 + 0.93 \times X_2 + 1.40 \times X_3 + 1.62 \times X_4 + 1.035 \times X_1X_2 - 3.20 \times X_1X_3 + 1.16 \times X_1X_4 - 1.44 \times X_2X_3 - 0.69 \times X_2X_4 + 2.36 \times X_3X_4 - 2.99 \times X_1^2 - 5.12 \times X_2^2 - 2.15 \times X_3^2 - 1.09 \times X_4^2$ (eqn (5))

Table 4 Optimized and predicted batch of SC-CS-NPs with independent variables and dependent variables

	Independent variables				Dependent variables				
Batch	X_1	X_2	X_3	X_4	Y_1	Y_2	Y_3	Y_4	Y_5
Predicted	0.15	0.15	800	5.0	99.24	0.351	40.98	41.14	79.21
Optimized	0.15	0.16	830	5.3	93.21 ± 3.31	0.317 ± 0.003	44.4 ± 2.93	41.23 ± 1.97	82.61 ± 4.93

Optimized dependent variables	Observed value	*p*-value	Entrapment efficiency (%)	Drug loading (%)	pH	Process yield (%)
Particle size	93.21 ± 3.31 nm	<0.0001	82.61 ± 4.93	41.23 ± 1.97	5.3 ± 0.16	83.58 ± 3.64
PDI	0.317 ± 0.003	<0.0001				
Zeta potential (mV)	+44.4 ± 2.93	<0.0001				

the enhancement in viscosity, which produces resistance against the attrition force of sonication, and ultimately particle agglomeration. An increase in sonication time results in a reduction in the particle size, which can be due to the droplets breaking through the higher mechanical energy against the viscous dispersed phase. We obtained a difference of 263.86 nm in particle size in between lower and higher concentration of CS and TPP for all the prepared formulations. The addition of TPP resulted in the emulsification and stabilization of the prepared formulation, which affected chitosan and the formation of particles. If the TPP concentration was maintained during the preparation of the new formulation, it was responsible for an increase in the surface area of the particles by breaking into the particles with a small size. Therefore, it is the most important parameter, *i.e.*, concentration of TPP and CS, affecting the particle size of the prepared novel formulation. The sonication time is a very important parameter decreasing the particle size by giving mechanical energy up to the minimum size, after which there was no possible reduction in particle size.

Zeta potential affected by independent variables

The stability of the particles in colloids was determined by ZP. It has been reported that a more positive ZP value for nanoparticles indicates more stable nanoparticles. The particles are attracted by van der Waals bonding, resulting in their aggregation due to their lower ZP. All the ZP results are shown in Tables 2–4. The average ZP value with the optimized value of TPP (0.16% w/v) and CS (0.15% w/v) was found to be +44.4 ± 2.93 mV at 830 rpm speed and pH 5.3. With an increased in the CS concentration, the ZP also increased, as shown in Fig. 1C. The polymer contains charge that can be controlled by the ZP of the prepared nanoparticles. Fig. 1C clearly indicates that the ZP charge on the nanoparticles is a significant criterion.

Effect of PDI on prepared nanoparticles

The increase or decrease in PDI is directly proportional to the stirring speed, CS (%), and TPP (%) of the final nanoparticles, as shown in eqn (2) and Fig. 1B.

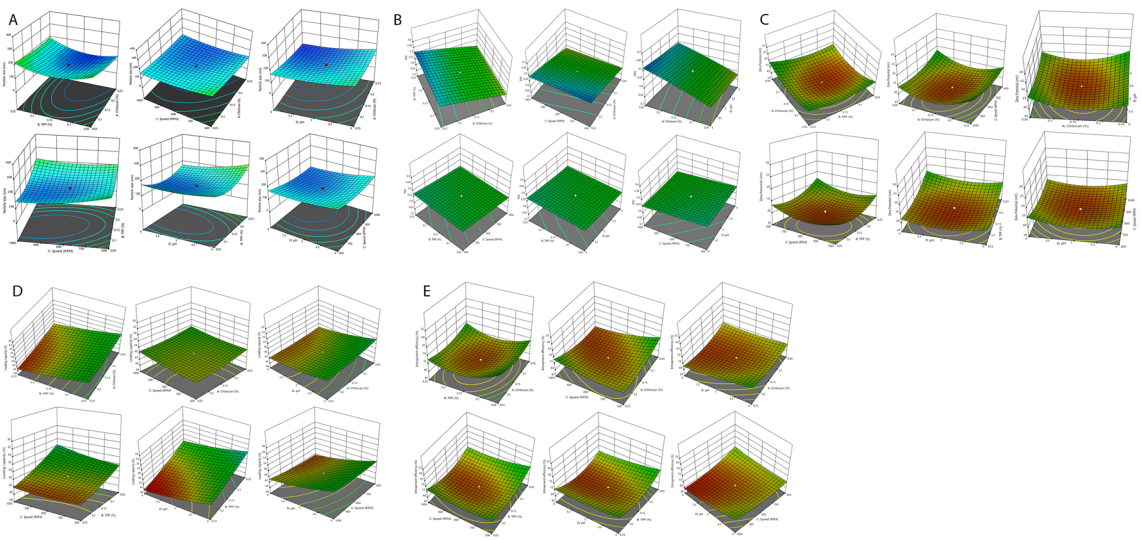

Fig. 1 (A) Response surface plot showing the effect of the dependent variables on the particle size. (B) Response surface plot showing the effect of the dependent variables the polydispersity index (PDI). (C) Response surface plot showing the effect of the dependent variables on the zeta potential. (D) Response surface plot showing the effect of dependent variables on the drug loading. (E) Response surface plot showing the effect of the dependent variables on the entrapment efficiency.

Optimization of entrapment efficiency by the optimization of independent variables and their effects on it

Table 2 shows all the data related to the optimization of EE for the prepared NPs. Tables 3 and 4 show all the factors evaluated and the significance of their impact. The effects of independent variables were determined on *S*-allyl cysteine entrapment for the preparation of nanoparticles, and also their response in the surface methodology calculated. With an increase in the quantity of CS and TPP, the EE of the prepared nanoparticles also increased (Fig. 1E). The increase in the EE of the prepared nanoparticles can be attributed to the enhancement in the polymer (%) resulting in an enhancement in SC entrapment with the minimization of SC diffusion due to the enhancement in viscosity. The reduction in particles size at the optimized stirring speed and pH was directly responsible for the EE of the NPs (Fig. 1E). This is due to the presence of the hydrophilic drug and the reduction in the size of the NPs *via* stirring speed (rpm). The surface-based responses were plotted with their combined effect (Fig. 1(A))(E). The results were found based on the direct relationship between the entrapment of *S*-allyl cysteine and an independent variable (stirring speed in rpm) in the response surface plot. An increase in the stirring speed in parallel with a reduction in the particle size finally enhanced the entrapment of the drug (EE). An increase in the concentration of CS polymer resulted in the maximum entrapment efficiency of *S*-allyl cysteine at the optimized stirring speed compared to a low concentration of CS polymer. A clear explanation was found based on the results of all the input variables and their impact on the entrapment of *S*-allyl cysteine. The relationship for the quadratic response was expressed *via* a regression equation and based on its coefficient. CCD gave a result based on the correlation of the quadratic between outcomes such as particle size and entrapment and linear factors such as zeta potential. The regression equation was projected for various levels (dependent and independent factors). Any modification in the factors was calculated correctly using this equation in the preparation of the nanoformulation simultaneously. Any interference effect of all independent variables was also helpful in all 5-dependent variables and their responses. The ZP (Y_3) analysis showed a value of >0.9894 (Table 3) for each regression equation, which was very close to the projected and adjusted Y_3 values for each response (Fig. 2). All these results suggest the statistical validity with the application of this regression equation for the optimization of SC CS NPs (Fig. 2).

The results were validated again based on the RSM of four check points ($X_1 : X_2 : X_3 : X_4$), *i.e.*; X_1 = chitosan (%), X_2 = TPP (%), X_3 = speed (rpm), and X_4 = pH (Table 5). All four check points ($X_1 : X_2 : X_3 : X_4$) were validated based on the results of the

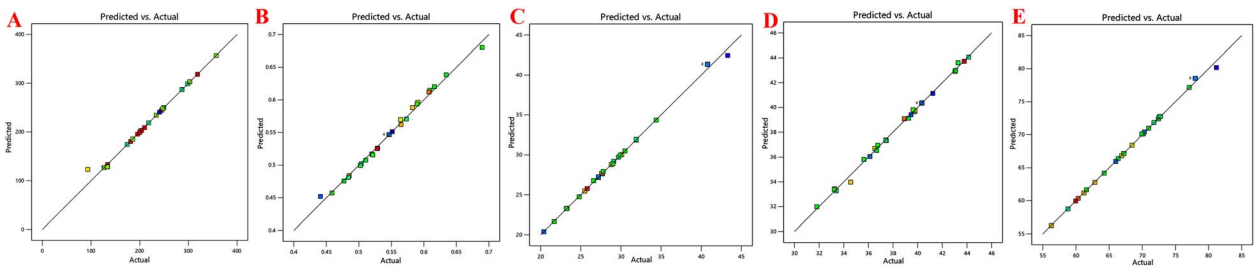

Fig. 2 Linear co-relation plot between the actual and predicted values of (A) average particle size (nm), (B) polydispersity index (PDI), (C) zeta potential (ZP: mV), (D) drug loading capacity (LC: %), and (E) entrapment efficiency (EE: %).

Table 5 Different checkpoint formulations, predicted and experimental values of response variables and % prediction error for CS NP formulations

#	Optimized check point composition ($X_1 : X_2 : X_3 : X_4$)	Response variable	Experimental values	Predicted values	Prediction error (%)
1	0.15 : 0.16 : 830 : 5.3	Y_1: PS: nm	93.21 ± 3.31	99.24	+3.16
		Y_2: PDI	0.317 ± 0.003	0.351	−2.27
		Y_3: ZP: mV	44.4 ± 2.93	40.98	+1.34
		Y_4: DL: %	41.23 ± 1.97	41.14	−0.62
		Y_5: EE: %	82.61 ± 4.93	79.21	+3.75
2	0.16 : 0.15 : 800 : 5.5	Y_1: PS: nm	147.34 ± 13.06	148.91	+0.57
		Y_2: PDI	0.450 ± 0.005	0.423	−1.64
		Y_3: ZP: mV	29.0 ± 1.57	28.91	+1.98
		Y_4: DL: %	39.62 ± 2.95	39.81	−0.39
		Y_5: EE: %	67.22 ± 3.91	67.15	+1.03
3	0.15 : 0.15 : 800 : 5.0	Y_1:PS: nm	165.71 ± 13.02	167.53	+2.38
		Y_2: PDI	0.473 ± 0.006	0.431	−2.18
		Y_3: ZP: mV	31.90 ± 2.79	31.94	+0.53
		Y_4: DL: %	37.41 ± 1.32	37.36	+1.32
		Y_5: EE: %	72.74 ± 5.46	72.76	−0.87

dependent variables, *i.e.*, Y_1 = particle size (PS: nm), Y_2 = polydispersity index (PDI), Y_3 = zeta potential (ZP: mV), Y_4 = loading capacity (DL: %), Y_5 = entrapment efficiency (EE: %), as mentioned in Table 5. It was again checked *via* Y_1: PS: nm, Y_2: PDI, Y_3: ZP: mV, Y_4: DL: %, Y_5: EE: %. The validation of RSM was examined the *via* % age-based prediction error calculation by comparing the experimental values with the predicted values of the obtained responses. All the responses were investigated *via* comparison of the predicted values with % age error of projection in the range of −2.27 to +3.75%. Our practical values were fitted with the theoretical values with very small prediction error. The optimization of SC CS NPs was confirmed *via* the maximum extrapolative ability of RSM design. The Design Expert® Software was employed for the optimization of SC CS NPs based on 4-independent variables applied to PS ≤ 93.21 ± 3.31 nm (or less than 100 nm). This value was fitted to brain targeting *via* i.n. drug delivery with +44.4 mV ZP, giving the highest EE with maximum stability. The CS NPs were prepared and optimized based on 5-dependent variables that indicated their predicted value with quadratic equations of different constraints through CCD design. This software was used to determine the optimized concentration of different compositions in w/v of 0.150% CS and 0.160% TPP, stirring speed of 830 ppm, and pH of 5.3 (Table 5).

The results were found based on the suggestion of CCD design for the optimized SC CS NPs, which were 0.150% w/v CS, 0.160% w/v TPP, stirring speed of 830 ppm, and pH of 5.3 (Table 3) based on 5-dependent variables and their predicted value with quadratic equations of different constraints. Additionally, 93.21 ± 3.31 nm PS, +44.4 ± 2.93 mV ZP, 0.317 ± 0.003 PDI, 41.23 ± 1.97% DL, and 82.61 ± 4.93% EE with 0.9925 regression were suggested for the opt-SC CS NPs. SC CS NPs were prepared and optimized based on the their predicted value and correlated with the practical value to validate the size of the SC nanoparticles, drug loading, EE, PDI, and ZP (Table 4, Fig. 3A and B). The most important point is for a water-soluble drug to cross the BBB to increase its brain bioavailability for ischemic brain treatment. SC CS NPs showed increased uptake in cells. Also, they showed a +ve ZP, which is very beneficial to provide easy adhesion and their transport. This is due to the electrostatic attractions between the +ve charged NPs and −ve charged cell membrane.[20] The optimized SC CS NPs were analysed to determine their size (<100.0 nm) (Fig. 4), and the same results were obtained using a Zetasizer (Fig. 3). It has already been proven in many studies that NPs possessing a size of <100.0 nm can easily cross the BBB *via* the transportation of olfactory neurons transcellularly to the brain with the help of numerous endocytic pathways of sustentacular or neuronal cells in the olfactory membrane.[36] The results showed that the DL was 41.23 ± 1.97%, whereas the EE was 82.61 ± 4.93%. Thus, *S*-allyl cysteine can be entrapped in the core of the optimized-CS NPs. CS showed mucoadhesive characteristics, which are helpful for brain targeting from the intranasal route to enhance the nasal staying of the drug in the nasal mucosa, and finally very helpful to improve the brain bioavailability.[21]

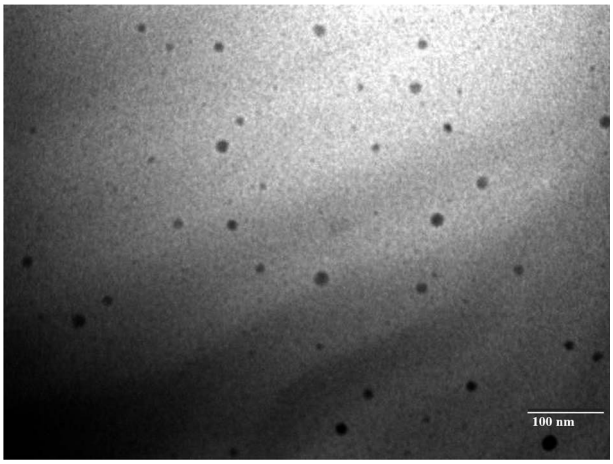

Fig. 4 Transmission electron microscopy (TEM) images of SC CS NPs.

Stability study for SC CS NPs

The stability of stored *S*-allyl cysteine chitosan nanoparticles (SC CS NPs) was assessed in pH 7.4 phosphate buffer at 4 °C (Table 6). Notably, there was only a minimal increase in particle size with time, with an insignificant response ($p > 0.05$) for changes in size observed at different sampling points. Initially, the particle size was 93.21 ± 3.31 nm in the stability trial, which

Fig. 3 Dynamic light scattering technique for determining the particle size distribution of mean particle size distribution curve (A) and zeta potential curve (B) of SC CS NPs.

Table 6 Storage stability studies for SC CS NPs at 4 °C for 6 months in pH 7.4 phosphate-buffered saline

Time (Months)	Mean particle size (nm) ± SD	Polydispersity index ± SD	Zeta potential (mV) ± SD	Entrapment efficiency (%) ± SD
0	93.21 ± 3.31	0.317 ± 0.003	44.4 ± 2.93	82.61 ± 4.93
1	98.26 ± 2.64	0.329 ± 0.005	42.61 ± 3.01	80.86 ± 4.01
3	103.64 ± 2.69	0.335 ± 0.009	41.64 ± 2.51	79.03 ± 3.14
6	126.84 ± 3.26	0.343 ± 0.018	38.15 ± 1.94	78.92 ± 3.43

increased to 126.84 ± 3.26 nm after 6 months of storage. Also, there was a slight change in the polydispersity index (PDI) of the SC CS NPs, with an acceptable increase in PDI from 0.317 ± 0.003 to 0.343 ± 0.018 during the stability trial, reaching ≤0.343 ± 0.018 PDI at the end of the trial. Additionally, there was only a minor alteration in the zeta potential (ZP) of the SC CS NPs, with a small decrease from 44.4 ± 2.93 mV to 38.15 ± 1.94 mV, which remained within the acceptable range for the optimized SC CS NPs, reaching 38.15 ± 1.94 mV ZP at the end of the trial. Furthermore, the encapsulation efficiency (%EE) of the SC CS NPs experienced a slight reduction, changing from 82.61 ± 4.93% to 78.92 ± 3.43%, which is also considered acceptable for the stability of the optimized SC CS NPs, with 78.92 ± 3.43% EE observed after 6 months of storage. In summary, our findings indicate that there were no significant changes that would impact our optimized nanoparticles, leading us to conclude that the stability of the optimized SC CS NPs was excellent throughout the 6 month storage period. We utilized a phosphate buffer at pH 7.4 and 4 °C to evaluate the stability of the optimized nanoparticles. In conclusion, all the assessed parameters, including nanoparticle size, zeta potential, encapsulation efficiency, and polydispersity index, demonstrated excellent storage stability for the optimized SC CS NPs. We observed a slight increase in particle size after 6 months of storage, which remained within an acceptable range.[31] Chitosan exhibited minimal swelling when suspended in phosphate buffer, which can be attributed to the increase in the size of the nanoparticles. The slight change in the PDI after 6 months of storage confirmed that the optimized nanoparticles did not aggregate, which is not a significant concern. The decrease in zeta potential observed at the end of the 6 month trial was likely due to the interaction between the positive charge of chitosan in the optimized SC CS NPs and the negative charge of the NH_2 groups. We attribute the minor increase in nanoparticle size over time to the surface interactions between these charges, affecting the zeta potential. A previous study also reported a substantial decrease in zeta potential after one month of storage.[37,38]

In vitro S-allyl cysteine release

The release of *S*-allyl cysteine from the opt-SC CS NPs was 79.92 ± 3.86% up to 24 h (Fig. 5A). The opt-SC CS NPs exhibited 40.21 ± 3.25% release of *S*-allyl cysteine up to 2 h because of the initial or first burst release and the biphasic behavior of the nanoformulation. SC was released from the surface (*i.e.*, SC was present in the highest quantity on the surface of SC CS NPs) in PBS solution as the dissolution medium exhibiting the maximum solubility at the time of burst release. The remaining quantity of *S*-allyl cysteine exhibited sustained released after 2 h. Finally, it was concluded that burst release occurred due to the existence of the highest quantity of SC on the surface of the opt-SC CS NPs. Now, it was clearly shown that the highest % of SC solubility depended on the release of SC due to their simultaneous quick dissolution. The most important point here to discuss is that the entrapment of SC inside the core of the CS NPs is directly related to the SC (drug) released in a sustained and controlled way. We can say the matrix system is the most important parameter, given that the drug (SC) was equally and homogenously dispersed in the matrix. Here, the emulsifying

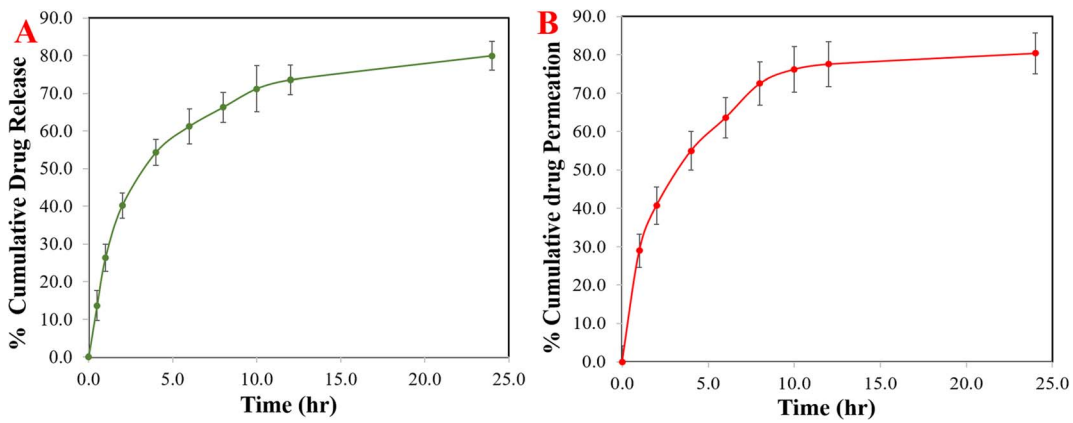

Fig. 5 The cumulative percentage release of *S*-allyl cysteine (SC) from SC CS NPs (A) and *ex vivo* permeation profiles of SC from optimized SC CS NPs at different intervals (B).

agent (*e.g.*, TPP) exhibited the highest emulsifying capacity, resulting in a homogenous mixture of *S*-allyl cysteine (drug). Therefore, it showed the delayed release of *S*-allyl cysteine.[21] Various models were applied to determine the coefficient of correlation (r^2), among which, the Higuchi model showed an r^2 value of 0.979, which is very close to the fitness of model. Therefore, the best-suited model was the Higuchi model for the opt-SC CS NPs. The Korsmeyer–Peppas equation was applied and a result of 0.969 was calculated using the equation $\log(M_t/M_\infty) = \log k + n \log t/2.303$, in which the exponential value (n) was between 0.43 and 0.84. Therefore, this is a clear sign the both diffusion and swelling controlled the release of *S*-allyl cysteine, indicating different means of transport.[1]

Nasal permeation

SC CS NPs exhibited great permeation of up to 80.36 ± 5.33 (Fig. 5B). The formulation of the SC CS NPs was optimized to determine the improvement in permeation *via* CS polymer, which showed >80.0% up to 24 h, *i.e.*, highest permeability to nasal mucosa. There was a great interaction between the +ve charged NH_2-group on the second position of carbon in CS and the −ve charge of the cell membranes. Therefore, the mechanism involved the tight junction permeability of the mucosal epithelial cells.[1] SC is a hydrophilic drug and shows very low permeability, which can be due to the absence of its interaction with the membrane of nasal mucosa. Richter and Keipert reported that a drug must be lipophilic to achieve the highest permeation in the nasal mucosa.[39] This suggests the permeation of the drug (SC) due to the low particle size of <100.0 nm and surface hydrophobicity of SC CS NPs, producing good partitioning in the biological membrane. Thus, it was concluded that based on the low size of the particles in the nanometer range of less than 100 nm, great EE%, maximum yield%, and great DL%, the permeation of the drug could easily increase, *i.e.*, SC from opt-SC CS NPs.

Development of LC-MS method for the evaluation of the PK parameters

Fig. 6A and B show the MS and MS/MS scans of *S*-allyl cysteine with A: blank brain homogenate, B: blank plasma, C: *S*-allyl cysteine (SC) extracted from brain homogenate, and D: plasma-extracted *S*-allyl cysteine (SC) [Fig. 7]. We found greater than 83.69% recovery for the plasma and brain homogenates. The developed method was linear with $r^2 > 0.997$ in both plasma and brain homogenates over the range of 5.0 to 1300.0 ng mL^{-1} for SC. *S*-Allyl cysteine showed all the peaks related to the extracted brain and plasma, which indicates the selectivity of the method. Table 7 presents the all data related to the inter- and intra-day precision and accuracy. All the results are summarized for all levels of QCs of *S*-allyl cysteine related to the intra and inter batch precision, which were calculated to be 2.43–4.38 and 2.44–4.24 in BH and PL, respectively. The % accuracy calculated as the intra and inter batch % accuracy was 96.21% to 99.06% and 96.00% to 98.87% for BH and PL, respectively (Table 7). All the stability results are summarized for *S*-allyl cysteine under all the storage conditions in Table 8.[1]

Pharmacokinetic study

All the parameters of PK were compared and analysed *via* the trapezoidal method (*e.g.* $-T_{max}$, $-C_{max}$, $-AUC_{0-t}$, $-K_{el}$, and $-t_{1/2}$), and also a graph concentration of *S*-allyl cysteine *vs.* time plotted (one-time dose was given *via* i.n. and i.v. for SC CS NPs

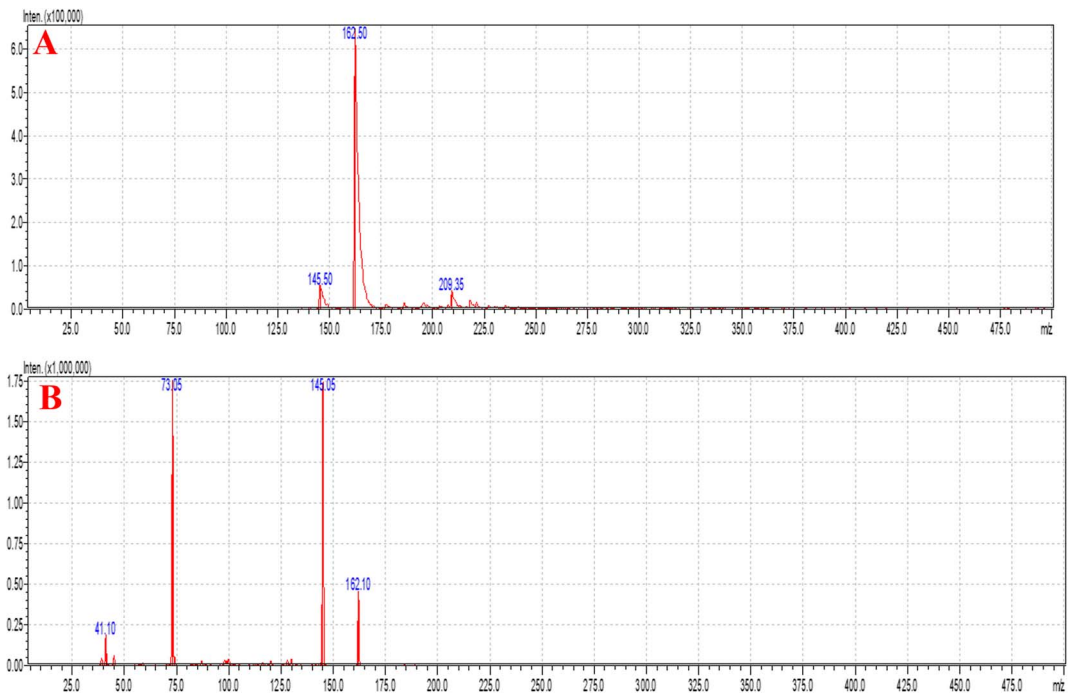

Fig. 6 Mass spectra of *S*-allyl cysteine, *i.e.*, MS scan (A) and MSMS scan (B).

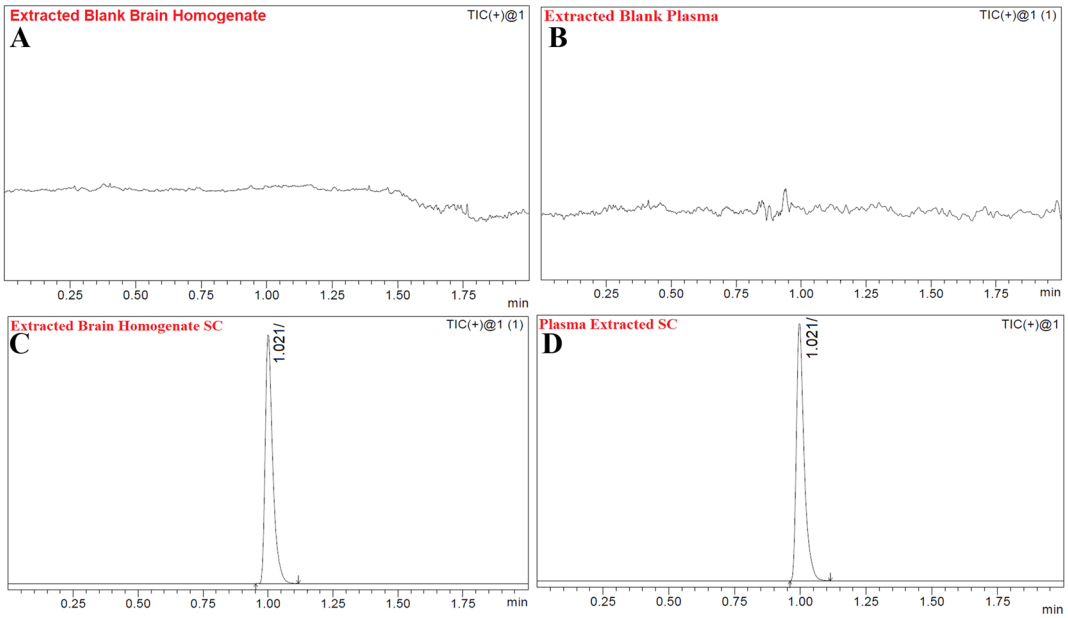

Fig. 7 Chromatograms of blank extracted brain homogenate (A), blank extracted plasma (B), extracted brain homogenate *S*-allyl cysteine (SC) (C), and plasma-extracted *S*-allyl cysteine (SC) (D).

and SC-S in animals) (Fig. 8). The results for C_{max} were found to be 66.47 ± 8.68 ng mL^{-1} (i.v.) and 119.34 ± 10.93 ng mL^{-1} (i.n. route) for SC-S and 219.64 ± 28.54 ng mL^{-1} (i.v. route) and 983.64 ± 65.82 ng mL^{-1} (i.n. route) for SC CS NPs. The results were found to be highly significant (***$p < 0.001$) for SC CS NPs compared to SC-S (Table 9) due to their sustained and controlled release of *S*-allyl cysteine. *S*-Allyl cysteine was enhanced in AUC_{0-t} (1052.08 ± 29.67 ng h mg^{-1}) for SC-S & AUC_{0-t} (12405.15 ± 91.53 ng h g^{-1}) for SC CS NPs. This is a clear indication of intranasal to brain targeting *via* our prepared and optimized SC CS NPs.[31]

Here, *S*-allyl cysteine was employed as a therapeutic agent and entrapped in the core of opt-NPs. The release of the drug is very important when it is delivered from a colloidal system to produce a proper physiological response. If there is a small modification of the physicochemical medium based on the characteristics of the NPs, it can optimize their release of *S*-allyl cysteine. *S*-allyl cysteine was encapsulated in opt-CS NPs, which was delivered through i.n. route to the brain, which also has a pH of 7.4. Here, the most important discussion is the enhancement of permeability and the staying time in the nasal mucosa, *i.e.*, EPR *via* i.n. route by the surface charge and size of opt-SC CS NPs, presenting a great approach to facilitate the permeation of SC based on the maximum retention time in the nasal mucosa, which helped to deliver SC to every cell in the brain. The charge of the NPs facilitated SC to target a particular place with the optimum release of SC (drug). A smaller particle size (less than 100 nm) resulted in a smooth path to enhance the

Table 7 Validation: precision and accuracy data for *S*-allyl cysteine (SC) in different biomatrices[a]

			Intra-batch precision			Inter-batch precision			
Biomatrix	Quality-control samples	Theoretical concentration (ng mL^{-1}) or (ng g^{-1})	Observed concentration (ng mL^{-1}) or (ng g^{-1}) ± SD	Accuracy[b] (%)	Precision[c] (CV%)	Observed concentration (ng mL^{-1}) or (ng g^{-1}) ± SD	Accuracy[b] (%)	Precision[c] (CV%)	Recovery[d] (%)
Brain homogenate	LOQQC	5.05	4.93 ± 0.12	97.62	2.43	4.91 ± 0.13	97.23	2.65	77.06
	LQC	14.50	13.95 ± 0.53	96.21	3.80	13.93 ± 0.54	96.07	3.88	80.34
	MQC	540.00	530.16 ± 17.41	98.18	3.28	528.62 ± 18.67	97.89	3.53	83.69
	HQC	1040.00	1027.14 ± 30.21	98.76	2.94	1020.94 ± 32.48	98.17	3.18	81.94
Plasma	LOQQC	5.05	4.94 ± 0.14	97.82	2.83	4.92 ± 0.12	97.43	2.44	78.31
	LQC	14.50	13.94 ± 0.61	96.10	4.38	13.92 ± 0.59	96.00	4.24	81.09
	MQC	540.00	527.61 ± 18.27	97.71	3.46	526.06 ± 19.01	97.42	3.61	83.66
	HQC	1040.00	1030.23 ± 29.42	99.06	2.86	1028.25 ± 27.94	98.87	2.72	80.24

[a] Values (mean ± SD) are derived from 6 replicates. [b] Accuracy (%) = mean value of [(mean observed concentration)/(theoretical concentration)] × 100. [c] Precision (%): coefficient of variance (percentage) = standard deviation divided by mean concentration found × 100; and. [d] Recovery (%) = mean value of (peak height (mV) obtained from extracted biological sample)/(peak height (mV) obtained from aqueous sample) × 100.

Table 8 Validation: stability data for *S*-allyl cysteine (SC) in different biomatrices[a,b]

	LQC (5.05 ng mL^{-1} or ng g^{-1})		MQC (540.0 ng mL^{-1} or ng g^{-1})		HQC (1040.0 ng mL^{-1} or ng g^{-1})	
Exposure condition	Brain homogenate	Plasma	Brain homogenate	Plasma	Brain homogenate	Plasma
Long term stability; recovery (ng) after storage (−80 °C)						
Previous day	4.98 ± 0.13	4.99 ± 0.11	531.01 ± 15.62	529.61 ± 15.34	1033.92 ± 26.01	1032.46 ± 25.15
30th day	4.81 ± 0.14 (96.56%)	4.85 ± 0.12 (97.19%)	515.63 ± 16.26 (97.10%)	513.26 ± 14.29 (96.91%)	1011.02 ± 23.11 (97.78%)	1013.68 ± 23.68 (98.18%)
Freeze–thaw stress; recovery (ng) after freeze–thaw cycles (−80 °C to 25 °C)						
Pre-cycle	4.99 ± 0.12	5.01 ± 0.12	535.05 ± 12.68	536.14 ± 16.21	1034.06 ± 27.03	1033.42 ± 26.14
First cycle	4.91 ± 0.13 (98.40%)	4.96 ± 0.11 (99.00%)	511.63 ± 16.49 (95.62%)	516.31 ± 15.34 (96.30%)	1021.11 ± 21.66 (98.75%)	1019.03 ± 25.10 (98.61%)
Second cycle	4.84 ± 0.12 (96.99%)	4.90 ± 0.12 (97.80%)	499.91 ± 15.61 (93.43)	498.21 ± 16.32 (92.93%)	1010.33 ± 23.54 (97.71%)	1008.79 ± 26.17 (97.62%)
Third cycle	4.75 ± 0.14 (95.19%)	4.84 ± 0.13 (96.61%)	491.29 ± 13.83 (91.82%)	489.95 ± 15.34 (91.38%)	1000.96 ± 24.36 (96.80)	1001.92 ± 25.21 (96.95%)
Benchtop stability; recovery (ng) at room temperature (25 °C)						
0 h	5.01 ± 0.11	4.97 ± 0.12	534.83 ± 15.32	535.28 ± 16.21	1036.23 ± 22.51	1035.25 ± 24.26
24 h	4.95 ± 0.13 (98.80%)	4.83 ± 0.11 (97.18%)	516.26 ± 14.25 (96.53%)	517.64 ± 15.28 (96.70%)	1018.21 ± 23.43 (98.26%)	1014.24 ± 23.02 (97.97%)
Post-processing stability; recovery (ng) after storage in an auto sampler (4 °C)						
0 h	5.01 ± 0.12	4.98 ± 0.13	533.21 ± 15.21	532.59 ± 16.08	1034.06 ± 23.01	1036.19 ± 24.65
4 h	4.96 ± 0.14 (99.00%)	4.81 ± 0.12 (96.59%)	519.29 ± 15.06 (97.39%)	518.37 ± 14.03 (97.33%)	1017.21 ± 22.61 (98.37%)	1021.64 ± 21.82 (98.60%)

[a] Values (mean ± SD) are derived from six replicates. Figures in parenthesis represent analyte concentration (%) relative to time zero. [b] Theoretical contents; LQC: 14.5 ng mL^{-1}; MQC: 540.00 ng mL^{-1}; and HQC: 1040.00 ng mL^{-1}.

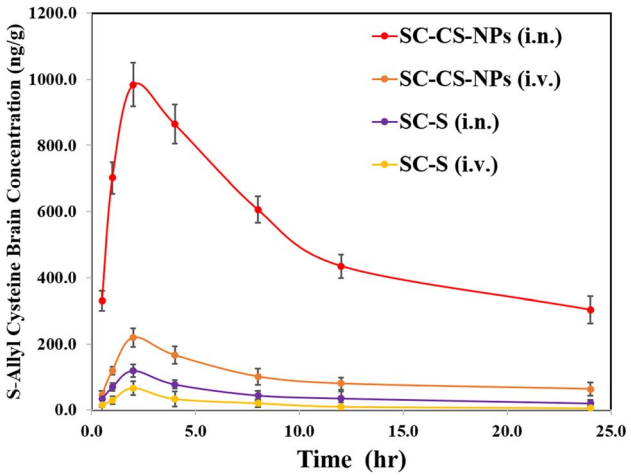

Fig. 8 Representation of pharmacokinetic results of *S*-allyl cysteine (SC) in the brain at various intervals after different routes of administration and their comparative study for SC CS NPs (i.n.) to SC CS NPs (i.v.), SC-S (i.n.), and SC-S (i.v.).

retention time of the NPs in the nasal mucosa for the delivery of the drug to the brain with the help of the particle charge, which also facilitated the optimum release of the drug at the targeted location. Our optimized NPs were used to prolong the nasal retention time, and also increase the delivery of entrapped *S*-allyl cysteine to the brain by passive targeting.

The release of *S*-allyl cysteine occurred through biodegradable polymeric CS NPs with the help of their pore mechanism, and also again through the absorption of SC on the surface of the CS NPs and diffusion. The desorption of SC on the surface of the CS NPs or we can say the degradation and erosion of the polymeric surface occurred.[21] *S*-Allyl cysteine was rapidly released by 26.37 ± 3.64% up to 2 h, followed by sustained released up to 24 h. The fast release of *S*-allyl cysteine occurred due to the burst release of opt-SC CS NPs up to 24 h based on the SC CS NP external surface covering (Fig. 5A).

Our opt-NPs showed r^2 of 0.979 for the kinetic release according to the Higuchi model due to the release of *S*-allyl cysteine *via* the methods of diffusion and swelling in a controlled way.[21] The opt-SC CS NPs showed a size in the nano range, *i.e.*, less than 100 nm, which could easily permeate the nasal mucosa, and also the +ve charge of the NH_2 group of CS interacted with the −ve charge of the nasal mucosal surface.[21] The mucoadhesive property of CS is due to its oligosaccharide chain of mucin in the presence or absence of SC as a drug entrapped in the CS NPs. CS interacts due to the presence of mucin in the maximum quantity, which increased the CS mucoadhesive strength.[21]

PD-study of cerebral ischemia of optimized-SC CS NPs

Examination of neurobehavioral parameters

Analysis by rotarod. Some signs of motor impairment function were seen in the MCAO rats because of their ischemic

Table 9 PK of *S*-allyl cysteine after i.n. and i.v. administration to rats at the dose of 15.0 mg kg^{-1} in brain and plasma ($n = 6$, mean ± SD)

Formulation administration	Sample	C_{max} (ng mL^{-1} g^{-1})	T_{max}	$t_{1/2}$ (h)	K_e (h^{-1})	AUC_{0-t} (ng min mL^{-1} g^{-1})
SC-S (i.n.)	Brain	119.34 ± 10.93	2.00	13.22 ± 1.09	0.05245 ± 0.00013	1052.08 ± 29.67
	Plasma	33.69 ± 2.96	0.50	6.72 ± 0.98	0.10318 ± 0.00023	163.50 ± 5.97
SC-S (i.v.)	Brain	66.47 ± 8.68	2.00	8.92 ± 1.17	0.07775 ± 0.0013	3092.05 ± 19.34
	Plasma	1187.64 ± 90.28	0.50	4.30 ± 0.41	0.16122 ± 0.00029	4529.65 ± 66.29
SC-CS-NPs (i.n.)	Brain	983.64 ± 65.82	2.00	21.70 ± 7.89	0.03195 ± 0.00017	12 405.15 ± 91.53
	Plasma	101.34 ± 6.16	2.00	8.78 ± 1.19	0.07898 ± 0.00015	874.60 ± 27.06
SC-CS-NPs (i.v.)	Brain	219.64 ± 28.54	2.00	28.54 ± 5.06	0.02429 ± 0.00016	2357.44 ± 67.29
	Plasma	1148.97 ± 101.06	1.00	12.67 ± 1.07	0.05470 ± 0.00014	13 097.75 ± 189.61
SC-S (i.n.)	Brain/Plasma	3.54	4.00	1.97	0.51	6.44
SC-S (i.v.)	Brain/Plasma	0.06	4.00	2.07	0.48	0.68
SC-CS-NPs (i.n.)	Brain/Plasma	9.68	1.00	2.47	0.41	14.20
SC-CS-NPs (i.v.)	Brain/Plasma	0.19	2.00	2.25	0.44	0.18

Comparative bioavailability[a] ($AUC_{i.n.}/AUC_{i.v.}$) (%)

Formulations	SC-S	SC-CS-NPs
Blood	3.61	6.67
Brain	34.03**	526.21***

[a] Parameters are derived using mean ± SEM values of 6 different estimations *$p < 0.05$, **$p < 0.01$, and ***$p < 0.01$.

brain. The results were calculated based on their pretreatment for MCAO + SC CS NPs the coordination of muscular movement compared to the induction of MCAO animals, *i.e.*, $p < 0.001$ and SC-S group, *i.e.*, $p < 0.05$. The coordination of muscular movement decreased significantly in the MCAO-induced animals it compared to the SHAM group, *i.e.*, $p < 0.001$ (Fig. 9A).

SMA examination. No neurological deficit was found in the SHAM. In contrast, the MCAO group animals exhibited higher neurological deficit according to the SMA examination. The MCAO group of animals did not movement and it was observed that their posture curved to the paretic side. We observed a significant loss of movement in the spontaneous motor in the MCAO groups of animals compared to the animals in the SHAM

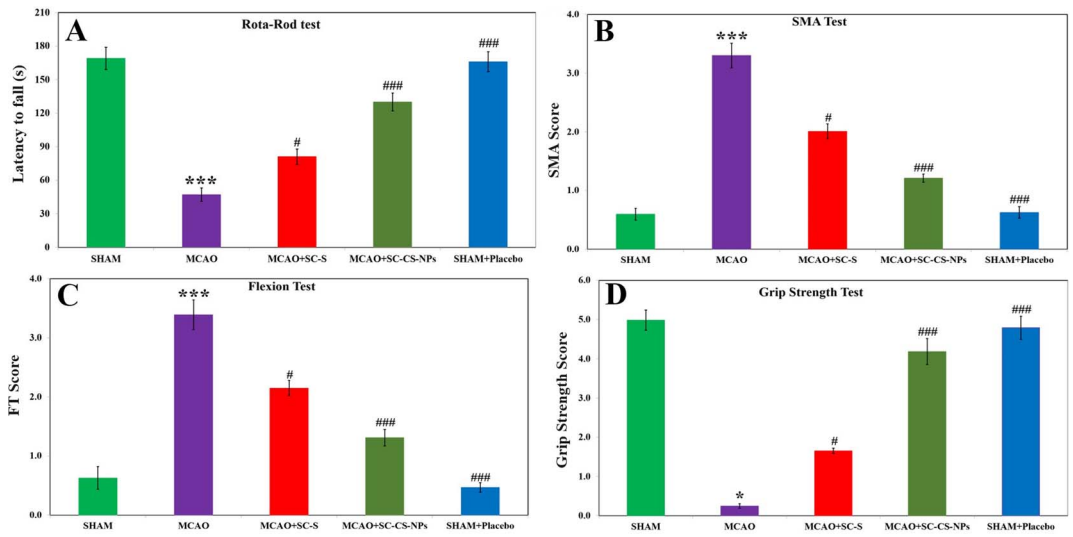

Fig. 9 Effect of SC-CS-NP pretreatment on TBARS content. TBARS content significantly increased in MCAO group compared to the SHAM group. Significance was determined as ***$p < 0.001$ compared with the SHAM group; $^{\#}p < 0.05$ and $^{\#\#\#}p < 0.001$ compared with the MCAO group. Shows effect of SC-CS-NPs on neurobehavioral deficits including rotarod (A), SMA (B), FT (C) and grip strength test for the control (SHAM) (D), ischemic (MCAO), SC-S (pure, 15 mg per kg b wt), SC-CS-NPs (15 mg per kg b wt), and substantial control: CS-NPs (Placebo) without SC (15 mg per kg b wt). Neurological deficit was significant in MCAO group in comparison to the control (SHAM) group. The animals treated with SC-CS-NPs had decreased neurological deficit. Values are expressed as mean ± SEM. Results from the comparison with the control group show a significant difference (***$p < 0.001$). Results obtained show a significant difference from MCAO-group ($^{\#}p < 0.05$ & $^{\#\#\#}p < 0.001$). The experiment was conducted for $n = 6$ data sets and results represented as mean ± SEM.

group ($p < 0.001$). We obtained significant results in the positive improvement score of SMA upon treatment with SC CS NPs, *i.e.*, $p < 0.001$, in the MCAO + SC CS NP group compared to the MCAO group. We also obtained highly improved neurological scores for SC CS NPs compared to the SC-S group, *i.e.*, $p < 0.05$. The scores of SMA related to SC-S were small compared to the MCAO + SC CS NP group (Fig. 9B).

Analysis based on flexion. In the analysis based on flexion, significantly greater scores in the MCAO rats, *i.e.*, $p < 0.001$, compared to SHAM were also obtained. The treatment of the MCAO group with SC CS NPs, *i.e.*, $p < 0.001$, resulted in a significant reduction in the neurological deficit score compared to the MCAO group rats. Also, the MCAO group treated with SC CS NPs showed a great improvement in neurological scores compared to the SC-S group, *i.e.*, $p < 0.05$ (Fig. 9C).

Grip strength analysis. A significant reduction in the grip strength ($p < 0.001$) was observed in the MCAO-induced-rats compared to the SHAM group of rats. Also, a highly significant results were found for the treatment of SC CS NPs in the MCAO group compared to the MCAO-induced animals, *i.e.*, $p < 0.001$. This resulted in an improvement in restoring neurological behavior very close to the SHAM group of animals, which was similar for the SC-S group, *i.e.*, $p < 0.05$ (Fig. 9D).

Evaluation of biochemical-related parameters

TBARS examination. The quantity of oxidative damage was examined using TBARS quantity examination. TBARS are a byproduct generated *via* lipid peroxidation and can be measured by the analysis of thiobarbituric acid. A significant result was found, *i.e.*, $p < 0.001$, for the amount of TBARS in the MCAO-induced animals compared to the animals in the SHAM group (Fig. 10). The TBARS content was reduced significantly [$p < 0.001$] in the rats in the ischemic model, *i.e.*, MCAO group was treated with opt-SC CS NPs compared to MCAO animals without treatment. SC CS NPs restored the TBARS concentration after the treatment of the MCAO rats, which was very close to the animals in the SHAM group. The MCAO group of animals treated with SC CS NPs had a greater reduction of TBARS concentration than the SC-S-treated animals (Fig. 10).

S-Allyl cysteine antioxidant effects on various enzymes. The activities of various enzymes (SOD, GR, GPx, and catalase) were reduced significantly ($p < 0.001$) in the MCAO model of ischemic rats compared to the SHAM group (Fig. 10). Treatment with *S*-allyl cysteine significantly enhanced ($p < 0.001$) the antioxidant activities of various enzymes, in which MCAO + SC CS NPs

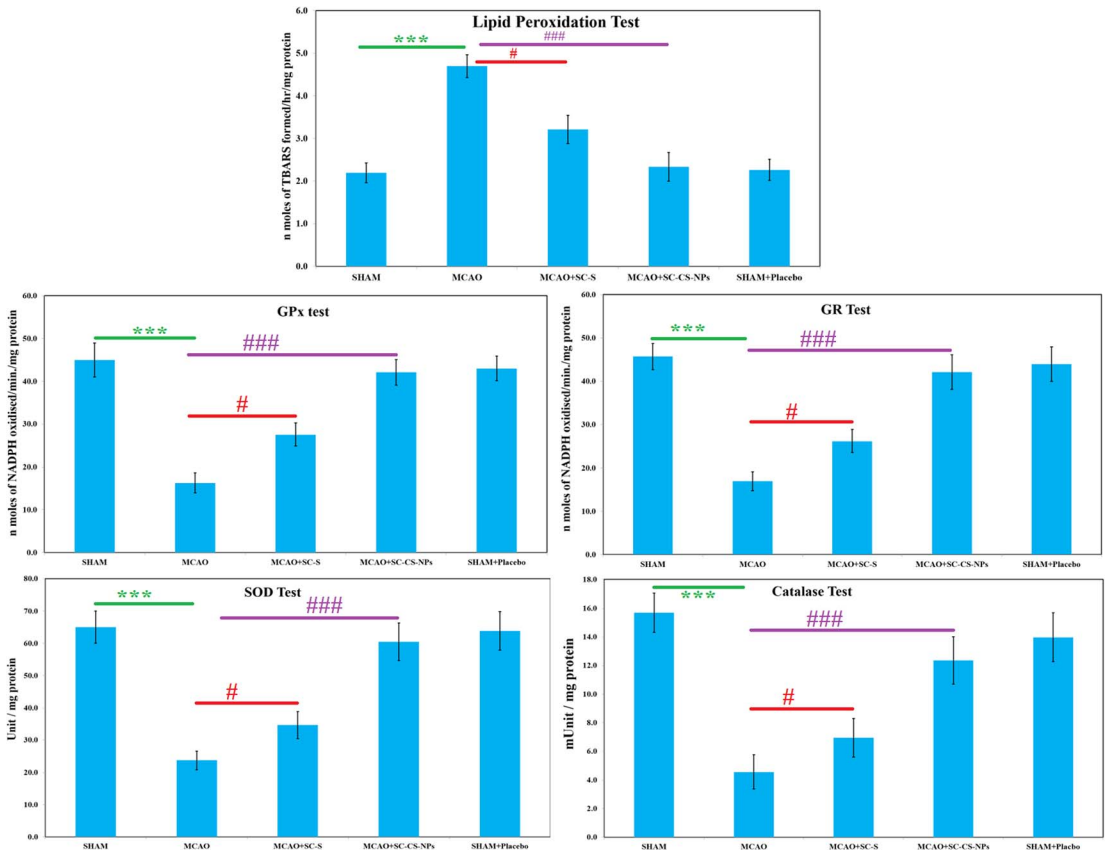

Fig. 10 Effect of *S*-allyl cysteine CS NP pre-treatment on TBARS concentration. TBARS amount was significantly enhanced in MCAO group compared to SHAM group. Significant results were evaluated as $^{***}p < 0.001$ compared to SHAM group; $^{\#}p < 0.05$ and $^{\#\#\#}p < 0.001$ compared with MCAO group. Effect of *S*-allyl cysteine CS NPs on the activity of various enzymes in different treatment groups. Results are displayed in the form of mean ± SEM of six animals. Significant results were found as $^{***}P < 0.001$ compared with SHAM group; $^{\#}P < 0.05$, $^{\#\#\#}P < 0.001$ compared to MCAO group.

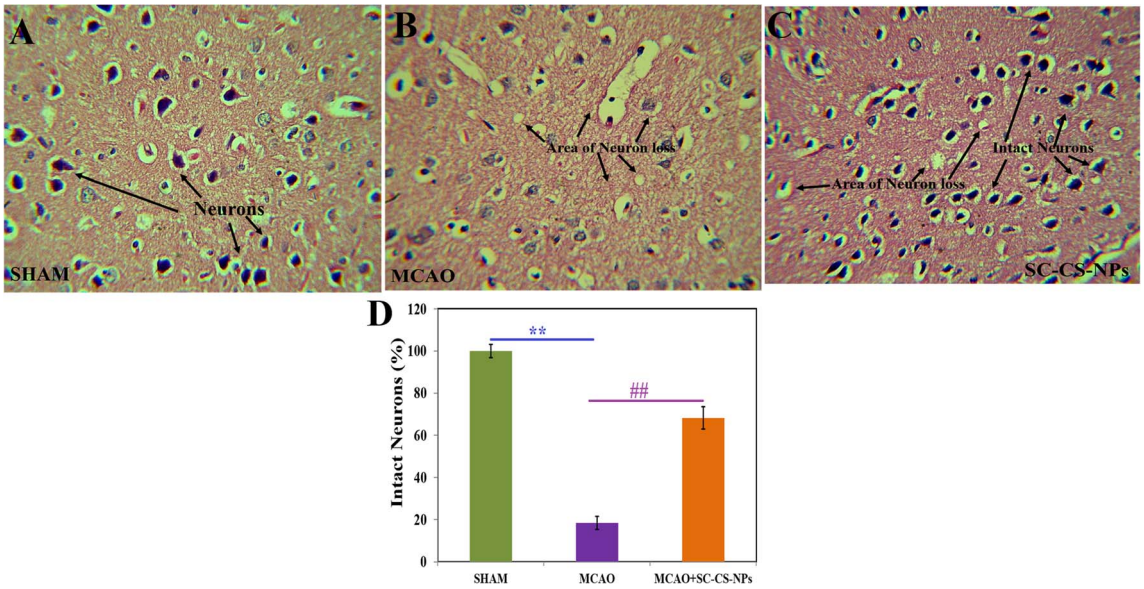

Fig. 11 Effect of SC-CS-NPs (15 mg kg^{-1}) on hematoxylin and eosin staining in the brain sections of the SHAM, MCAO, and MCAO + SC-CS-NPs. (A) Cortical area of SHAM group animal showed uniform distribution of neurons. Normal neurons with the characteristic conical outlines with no abnormal features are seen. (B) Tissues around infarcted area in the MCAO group show a focal area of vacuolation and neuronal loss. (C) Group of MCAO + SC-CS-NP rats shows partial neuronal loss. (D) Quantification of neuronal damage of SHAM, MCAO and MCAO + SC-CS-NPs rats. Original magnification ×20 and scale bar = 20 μm.

showed $p < 0.001$ compared to the MCAO ischemic animal group. MCAO + SC CS NPs produced the maximum concentration of all the antioxidant activities of the various enzymes.

Histopathological examination of various groups. Hematoxylin and eosin were used to stain the brain after one hour of MCAO in various groups for histopathological examination, followed by 24 h of reperfusion (Fig. 11). The frontal cortex part of the sectioned brain was collected to evaluate any alteration in the histopathology of the treated brain. No alteration in the pathology of the neurons was found, indicating that the brain was normal in the SHAM group. There was a loss in neurons including vacuolated spaces found in the histopathological brain slides of the MCAO-induced animals. The treatment of the MCAO groups of animals with SC CS NPs resulted in a small loss of neurons, and also vacuolated spaces between the intact neurons followed by histopathological restoration, which was very close to the SHAM group.

Presently, drug targeting *via* i.n. to the brain using nanoformulations to improve the bioavailability of drugs in the brain is common. However, many challenges still need to be addressed including the BBB as the main obstacle and some other obstacles.[1] Herein, we developed novel and optimized SC CS NPs to enhance the brain bioavailability of *S*-allyl cysteine administered *via* the i.n. route. To date, this is a first time opt-SC CS NPs were used in a developed MCAO model of rats *via* the i.n. route. SC CS NPs possess mucoadhesive nature to treat MCAO rats *via* the i.n. route. Consequently, the *S*-allyl cysteine staying time was prolonged in the nasal mucosa, indicating that CS acts as a strong mucoadhesive agent, which increases the rate of SC permeation, followed by enhancing its bioavailability in the brain.[31] SC was entrapped in CS NPs in their core, which is very helpful to protect it from chemical and extracellular transport by P-glycoprotein effluxion and biological environment. Opt-SC CS NPs enhanced the bioavailability of SC in the brain due to the stronger transcellular transport of SC by the olfactory-neurons into the brain *via* the endocytic pathway.[19]

The C_{max} (983.64 ± 65.82 ng g^{-1}) and AUC (12405.15 ± 91.53 ng min g^{-1}) increased significantly *via* the i.n. administration of SC CS NPs compared to *S*-allyl cysteine S (i.n.) and *S*-allyl cysteine S (i.v.) in the brain due to its transport directly by the olfactory lobe route to the brain, bypassing the BBB. CS has a mucoadhesive nature, which was also helpful to deliver *S*-allyl cysteine to the brain *via* a reduction in the clearance of SC *via* mucociliary in the normal environment. The *S*-allyl cysteine CS NPs (i.n.) enhanced the concentration of *S*-allyl cysteine in the brain for C_{max} (14.8 times) and AUC_{0-t} (4.01 times), which resulted in a greater increment in the concentration of SC compared to SC S *via* the i.v. route delivery. Based on the results, we concluded that the uptake of *S*-allyl cysteine in the brain *via* the nasal mucosa occurred *via* two different pathways, as follow: (1) systemic pathway: the drug was easily absorbed after reaching the systemic circulation, and then uptake by the brain by crossing the BBB. (2) Olfactory pathway: the drug was partially uptake into brain by the i.n. route.[1,2] Finally, it was observed that *S*-allyl cysteine CS NPs and SC-S had significantly high bioavailability in brain from the i.n. route compared to the other route, clearly indicating brain targeting *via* the i.n. route, which was also reported before (Table 9).[19] Finally, we concluded that the i.n. route is the main route to target the brain directly.[31] Our group also reported before that the same route was used to enhance the bioavailability of curcuminoids in the brain *via* PNIPAM NPs as a tool to deliver drugs.[3] PNIPAM NPs were also used to deliver curcumin and enhancement of its uptake compared to the simple suspension form of curcumin.[2]

This was due to the mucoadhesive nature of PNIPAM NPs with their maximum nasal staying time after opening of the tight junction of the membrane with an improvement in permeation, together with the sustained delivery of curcumin to the brain. Similarly, our proposed research used *S*-allyl cysteine CS NPs to deliver *S*-allyl cysteine *via* the i.n. route to the brain and improve its bioavailability. This is consistent with the previously reported study.

Here, a very sensitive and effective (up to the nanogram level) novel bioanalytical LC MS method was developed and successfully applied to examine the various parameters of PK and biodistribution in the brain and plasma in a comparative way. This is a great achievement in terms of the short time to analyze the samples with an economical application, which was validated successfully. *S*-Allyl cysteine was encapsulated in the opt-CS NPs with their mucoadhesive property successfully treating brain ischemic stroke in a MCAO model of ischemia in rats. *S*-Allyl cysteine CS NPs exhibited a significant protection and improvement in the neurological dysfunction, motor impairment, ischemia of brain, and alteration in correlation with biochemical parameters. We already successfully developed and validated a method for determining *S*-allyl cysteine in plasma. Herein, we developed this method for the quantification of *S*-allyl cysteine in the plasma and brain.[40]

Some neurological dysfunction and motor impairment were found based on different behavioral output parameters upon the examination of the animals in the MCAO group. The dysfunction of motor nerves started to destroy the pyramidal areas and motor cortex present in the MCAO area, followed by irrecoverable loss of synaptic activity in the motor cortex area and electrical activity obstruction in the subcortical area.[41] Free radicals are the main factor resulting in deficits of neurobehavioral induction *via* the production of oxidative stress.[42] We did not observe good results for the ischemic animal group in terms of neurobehavioral behavior, which can be attributed to the greater production of free radicals, altering the coordination of motor and locomotion because of the introduction of a necrotic effect in the sensory-motor cortices and caudate-putamen.[43] This regulated all the motor and sensorimotor actions. The results related to grip strength and rotarod were significant in the coordination of motor and locomotion in the MCAO model of animals. We also found the same findings for SMA examination. *S*-Allyl cysteine CS NPs were given by i.n. route, resulting in an excellent improvement in restoring neurobehavioral changes compared to the free *S*-allyl cysteine-S treated groups.

Oxidative stress causes changes in the biochemical composition in an ischemic brain after injury. Free radicals are produced after their massive burst production, which play a key role in neuronal injury because of their high reaction and size, causing cellular damage. Furthermore, lipid peroxidation occurs by ROS attacking the lipid-rich membranes.[2] Here, we found that the results were related to LPO due to the massive quantity of TBARS. This occurred because of the excitability of neurons in the initial stage of post-ischemic injury, resulting in the maximum collection of extracellular fluid glutamate. The free radicals produced in excess after cerebral ischemia injury produce oxidative injury to a large quantity of lipids and proteins in the membrane. The results showed that the activity of the SOD, GPx, GR, and catalase enzymes was affected by oxidative stress. It was reported that 6-gingerol pretreatment showed the opposing effect of enhancing oxidative stress.[1] Encapsulation of *S*-allyl cysteine in the *S*-allyl cysteine CS NPs enhanced the effect of *S*-allyl cysteine pretreatment. The neuronal cells were damaged due to the overproduction of superoxide radicals and formation of their derivatives after the cerebral ischemia damage. SOD produced the maximum number of free radicals after the ischemic brain reperfusion. SOD is a tool that can be used in the prevention of oxidative stress by the anions of superoxide catalytic dismutation to hydrogen per oxide. All the antioxidant enzymes (SOD, GPx, GR, and catalase) combined will result in the protection of the cells that are contact with O_2.[44] O_2 and H_2O_2 are converted to H_2O due to the presence of catalase enzyme. Histopathological alterations in the brain cells, *e.g.*, neuron swelling, loss of neurons, and vacuolation, were observed in the MCAO-induced animals. *S*-Allyl cysteine was given to improve the above-mentioned histopathological changes in the ischemic brain cells.

Conclusion

S-Allyl cysteine was encapsulated in optimized chitosan nanoparticles (opt-CS NPs) through the ionotropic gelation method. Central composite design (CCD) was employed to optimize the formulation of *S*-allyl cysteine chitosan nanoparticles (SC CS NPs) using a four-factor and five-level CCD design. The optimization criteria included drug loading (DL), encapsulation efficiency (EE), and particle size. The developed *S*-allyl cysteine CS NPs exhibited the controlled and sustained release of *S*-allyl cysteine for up to 24 h. The SC CS NPs also demonstrated a prolonged nasal retention time and high tolerability. The intranasal (i.n.) route of drug delivery allowed for the direct delivery of SC to the brain, bypassing the first-pass hepatic metabolism. The positive zeta potential (+ve ZP) in the optimized SC CS NPs indicated their stability, which is attributed to the presence of chitosan. Moreover, the SC CS NPs significantly improved the brain bioavailability of *S*-allyl cysteine, achieving effective results with a minimal dose compared to a simple *S*-allyl cysteine suspension (SC-S). These nanoparticles were assessed using the Longa *et al.* model of an ischemic brain, evaluating the neurobehavioral, biochemical, and histopathological aspects of ischemic brain conditions. The use of *S*-allyl cysteine CS NPs proved to be a safe and effective treatment *via* targeted intranasal drug delivery for cerebral ischemia. In the future, *S*-allyl cysteine CS NPs hold promise for large-scale applications in ischemic brain treatment, although comprehensive clinical studies on a larger scale will be necessary.

Conflicts of interest

The authors do not have any conflicts.

Acknowledgements

This study received financial support from Prince Sattam bin Abdulaziz University, Alkharj, Saudi Arabia, under grant PSAU/2023/R/1445. The authors extend their appreciation to the Deanship of Scientific Research & Innovation, Ministry of Education in Saudi Arabia for funding this research through the project number IFP-IMSUI-2023063. The authors also appreciate the Deanship of Scientific Research at Imam Mohammad ibn Saud Islamic University (IMSIU) for supporting this project. All the authors express their gratitude to the Animal House at the Institute for Research and Medical Consultations (IRMC), Imam Abdulrahman Bin Faisal University, Dammam, Kingdom of Saudi Arabia.

References

1 N. Ahmad, R. Ahmad, A. A. Naqvi, M. A. Alam, M. Ashafaq, M. Samim, Z. Iqbal and F. J. Ahmad, Rutin-encapsulated chitosan nanoparticles targeted to the brain in the treatment of Cerebral Ischemia, *Int. J. Biol. Macromol.*, 2016, **91**, 640–655.

2 N. Ahmad, R. Ahmad, M. Amir, M. A. Alam, A. Ali, A. Ahmad and A. Kamran, Ischemic brain treated with 6-gingerol loaded mucoadhesive nanoemulsion via intranasal delivery and their comparative pharmacokinetic effect in brain, *J. Drug Delivery Sci. Technol.*, 2021, **61**, 102130, DOI: **10.1016/j.jddst.2020.102130**.

3 N. Ahmad, S. Umar, M. Ashafaq, M. Akhtar, Z. Iqbal, M. Samim and F. J. Ahmad, A comparative study of PNIPAM nanoparticles of curcumin, demethoxycurcumin, and bisdemethoxycurcumin and their effects on oxidative stress markers in experimental stroke, *Protoplasma*, 2013, **250**(6), 1327–1338.

4 M. Ashafaq, S. S. Raza, M. M. Khan, A. Ahmad, H. Javed, M. E. Ahmad, R. Tabassum, F. Islam, M. S. Siddiqui, M. M. Safhi and F. Islam, Catechin hydrate ameliorates redox imbalance and limits inflammatory response in focal cerebral ischemia, *Neurochem. Res.*, 2012, **37**(8), 1747–1760.

5 M. Ashafaq, M. M. Khan, S. Shadab Raza, A. Ahmad, G. Khuwaja, H. Javed, A. Khan, F. Islam, M. S. Siddiqui, M. M. Safhi and F. Islam, S-allyl cysteine mitigates oxidative damage and improves neurologic deficit in a rat model of focal cerebral ischemia, *Nutr. Res.*, 2012, **32**(2), 133–143.

6 H. Tabassum, M. Ashafaq, S. Parvez and S. Raisuddin, Role of melatonin in mitigating nonylphenol-induced toxicity in frontal cortex and hippocampus of rat brain, *Neurochem. Int.*, 2017, **104**, 11–26.

7 E. Z. Longa, P. R. Weinstein, S. Carlson and R. Cummins, Reversible middle cerebral artery occlusion without craniectomy in rats, *Stroke*, 1989, **20**(1), 84–91, DOI: **10.1161/01.str.20.1.84**.

8 P. D. Maldonado, D. Barrera, I. Rivero, R. Mata, O. N. Medina-Campos, R. Hernández-Pando and J. Pedraza-Chaverrí, Antioxidant S-allylcysteine prevents gentamicin-induced oxidative stress and renal damage, *Free Radical Biol. Med.*, 2003, **35**(3), 317–324.

9 E. Garcia, D. Limon, V. Perez-De La Cruz, M. Giordano, M. Diaz-Muñoz, P. D. Maldonado, M. N. Herrera-Mundo, J. Pedraza-Chaverri and A. Santamaria, Lipid peroxidation, mitochondrial dysfunction and neurochemical and behavioural deficits in different neurotoxic models: protective role of S-allylcysteine, *Free Radical Res.*, 2008, **42**(10), 892–902.

10 H. Javed, M. M. Khan, A. Khan, K. Vaibhav, A. Ahmad, G. Khuwaja, M. E. Ahmed, S. S. Raza, M. Ashafaq, R. Tabassum, M. S. Siddiqui, O. M. El-Agnaf, M. M. Safhi and F. Islam, S-allyl cysteine attenuates oxidative stress associated cognitive impairment and neurodegeneration in mouse model of streptozotocin-induced experimental dementia of Alzheimer's type, *Brain Res.*, 2011, **1389**, 133–142.

11 F. Atif, S. Yousuf and S. K. Agrawal, S-allyl L-cysteine diminishes cerebral ischemia–induced mitochondrial dysfunctions in hippocampus, *Brain Res.*, 2009, **1265**, 128–137.

12 J. M. Kim, N. Chang, W. K. Kim and H. S. Chun, Dietary S-allyl-L-cysteine reduces mortality with decreased incidence of stroke and behavioral changes in stroke-prone spontaneously hypertensive rats, *Biosci., Biotechnol., Biochem.*, 2006, **70**, 1969–1971.

13 E. García, J. Villeda-Hernández, J. Pedraza-Chaverrí, P. D. Maldonado and A. Santamaría, S-allylcysteine reduces the MPTP-induced striatal cell damage via inhibition of pro-inflammatory cytokine tumor necrosis factor-α and inducible nitric oxide synthase expressions in mice, *Phytomedicine*, 2010, **18**(1), 65–73.

14 Y. Numagami, S. Sato and S. T. Ohnishi, Attenuation of rat ischemic brain damage by aged garlic extracts: a possible protecting mechanism as antioxidants, *Neurochem. Int.*, 1996, **29**, 135–143.

15 F. Pérez-Severiano, M. Rodríguez-Pérez, J. Pedraza-Chaverrí, P. D. Maldonado, O. N. Medina-Campos, A. Ortíz-Plata, A. Sánchez-García, J. Villeda-Hernández, S. Galván-Arzate, P. Aguilera and A. Santamaría, S-Allylcysteine, a garlic-derived antioxidant, ameliorates quinolinic acid-induced neurotoxicity and oxidative damage in rats, *Neurochem. Int.*, 2004, **45**(8), 1175–1183.

16 F. Pérez-Severiano, R. Salvatierra-Sánchez, M. Rodríguez-Pérez, E. Y. Cuevas-Martínez, J. Guevara, D. Limón, P. D. Maldonado, O. N. Medina-Campos, J. Pedraza-Chaverrí and A. Santamaría, S-Allyl cysteine prevents amyloid-beta peptide-induced oxidative stress in rat hippocampus and ameliorates learning deficits, *Eur. J. Pharmacol.*, 2004, **489**(3), 197–202.

17 Y. Ito, M. Ito, N. Takagi, H. Saito and K. Ishige, Neurotoxicity induced by amyloid beta-peptide and ibotenic acid in organotypic hippocampal cultures: protection by S-allyl-L-cysteine, a garlic compound, *Brain Res.*, 2003, **985**(1), 98–107.

18 N. Ahmad, R. Ahmad, A. A. Naqvi, M. A. Alam, M. Ashafaq, R. Abdur Rub and F. J. Ahmad, Intranasal delivery of quercetin-loaded mucoadhesive nanoemulsion for

treatment of cerebral ischaemia, *Artif. Cells, Nanomed., Biotechnol.*, 2018, **46**(4), 717–729.

19 N. Ahmad, M. S. Khalid, A. M. Al Ramadhan, *et al.*, Preparation of melatonin novel-mucoadhesive nanoemulsion used in the treatment of depression, *Polym. Bull.*, 2023, **80**, 8093–8132.

20 R. Fernandez-Urrusuno, D. Romani and D. Calvo, Development of a Freeze Dried Formulation of Insulin-Loaded Chitosan Nanoparticles Intended for Nasal Administration, *STP Pharma Sci.*, 1999, **9**, 429–436.

21 S. Md, R. A. Khan, G. Mustafa, K. Chuttani, S. Baboota, J. K. Sahni and J. Ali, Bromocriptine loaded chitosan nanoparticles intended for direct nose to brain delivery: pharmacodynamic, pharmacokinetic and scintigraphy study in mice model, *Eur. J. Pharm. Sci.*, 2013, **48**(3), 393–405.

22 N. Ahmad, Rasagiline-encapsulated chitosan-coated PLGA nanoparticles targeted to the brain in the treatment of parkinson's disease, *J. Liq. Chromatogr. Relat. Technol.*, 2017, **40**(13), 677–690.

23 C. Losa, M. J. Alonso, J. L. Vila, F. Orallo, J. Martinez, J. A. Saavedra and J. C. Pastor, *J. Ocul. Pharmacol.*, 1992, **8**(3), 191–198.

24 M. M. Badran, M. M. Mady, M. M. Ghannam and F. Shakeel, Preparation and Characterization of Polymeric Nanoparticles Surface Modified with Chitosan for Target Treatment of Colorectal Cancer, *Int. J. Biol. Macromol.*, 2017, **95**, 643–649.

25 N. Ahmad, R. Ahmad, M. A. Alam and F. J. Ahmad, Quantification and Brain Targeting of Eugenol-Loaded Surface Modified Nanoparticles Through Intranasal Route in the Treatment of Cerebral Ischemia, *Drug Res.*, 2018, **68**(10), 584–595.

26 T. Matsutomo, T. D. Stark and T. Hofmann, Targeted screening and quantitative analyses of antioxidant compounds in aged-garlic extract, *Eur. Food Res. Technol.*, 2018, **244**, 1803–1814, DOI: **10.1007/s00217-018-3092-6**.

27 S. Kim, S.-L. Park, S. Lee, S.-Y. Lee, S. Ko and M. Yoo, UPLC/ESI-MS/MS analysis of compositional changes for organosulfur compounds in garlic (Allium sativum L.) during fermentation, *Food Chem.*, 2016, **211**, 555–559, DOI: **10.1016/j.foodchem.2016.05.102**.

28 Q. Zhu, K. Kakino, C. Nogami, K. Ohnuki and K. Shimizu, An LC-MS/MS-SRM Method for Simultaneous Quantification of Four Representative Organosulfur Compounds in Garlic Products, *Food Anal. Methods*, 2016, **9**, 3378–3384, DOI: **10.1007/s12161-016-0535-1**.

29 T. Park, J.-H. Oh, J. H. Lee, S. C. Park, Y. P. Jang and Y.-J. Lee, Oral Administration of (S)-Allyl-L-Cysteine and Aged Garlic Extract to Rats: Determination of Metabolites and Their Pharmacokinetics, *Planta Med.*, 2017, **83**(17), 1351–1360, DOI: **10.1055/s-0043-111895**.

30 P. Calvo, C. Remuñan-López, J. L. Vila-Jato and M. J. Alonso, Chitosan and chitosan/ethylene oxide-propylene oxide block copolymer nanoparticles as novel carriers for proteins and vaccines, *Pharm. Res.*, 1997, **14**(10), 1431–1436, DOI: **10.1023/a:1012128907225**.

31 N. Ahmad, M. J. A. Al-Ghamdi, H. S. M. Alnajjad, B. B. A. Al Omar, M. F. Khan, Z. S. Al malki, A. A. Al Bassam, Z. Ullah, M. S. Khalid and K. Ashraf, A comparative brain Toxico-Pharmacokinetics study of a developed tannic acid nanoparticles in the treatment of epilepsy, *J. Drug Delivery Sci. Technol.*, 2022, **76**, 103772, DOI: **10.1016/j.jddst.2022.103772**.

32 M. A. Kelly, M. Rubinstein, T. J. Phillips, C. N. Lessov, S. Burkhart-Kasch, G. Zhang, J. R. Bunzow, Y. Fang, G. A. Gerhardt, D. K. Grandy and M. J. Low, Locomotor activity in D2 dopamine receptor-deficient mice is determined by gene dosage, genetic background, and developmental adaptations, *J. Neurosci.*, 1998, **18**, 3470–3479, DOI: **10.1523/JNEUROSCI.18-09-03470.1998**.

33 K. Vaibhav, P. Shrivastava, H. Javed, A. Khan, M. E. Ahmed, R. Tabassum, M. M. Khan, G. Khuwaja, F. Islam, M. S. Siddiqui, M. M. Safhi and F. Islam, Piperine suppresses cerebral ischemia-reperfusion-induced inflammation through the repression of COX-2, NOS-2, and NF-κB in middle cerebral artery occlusion rat model, *Mol. Cell. Biochem.*, 2012, **367**, 73–84, DOI: **10.1007/s11010-012-1321-z**.

34 J. Mohandas, J. J. Marshall, G. G. Duggin, J. S. Horvath and D. J. Tiller, Differential distribution of glutathione and glutathione-related enzymes in rabbit kidney. Possible implications in analgesic nephropathy, *Biochem. Pharmacol.*, 1984, **33**, 1801–1807, DOI: **10.1016/0006-2952(84)90353-8**.

35 M. M. Bradford, A rapid and sensitive method for the quantitation of microgram quantities of protein utilizing the principle of protein-dye binding, *Anal. Biochem.*, 1976, **72**, 248–254, DOI: **10.1016/0003-2697(76)90527-3**.

36 A. Mistry, S. Stolnik and L. Illum, Nanoparticles for direct nose-to-brain delivery of drugs, *Int. J. Pharm.*, 2009, **379**, 146–157.

37 M. Luangtana-Anan, S. Limmatvapirat, J. Nunthanid, R. Chalongsuk and K. Yamamoto, Polyethylene glycol on stability of chitosan microparticulate carrier for protein, *AAPS PharmSciTech*, 2010, **11**(3), 1376–1382, DOI: **10.1208/s12249-010-9512-y**.

38 M. A. Hibah, N. A. Alhakamy, R. Padder, M. Husain and S. Md, Preparation and characterization of chitosan coated PLGA nanoparticles of resveratrol: improved stability, antioxidant and apoptotic activities in H1299 lung cancer cells, *Coatings*, 2020, **10**, 439, DOI: **10.3390/coatings10050439**.

39 T. Richter and S. Keipert, In vitro permeation studies comparing bovine nasal mucosa, porcine cornea and artificial membrane: androstenedione in microemulsions and their components, *Eur. J. Pharm. Biopharm.*, 2004, **58**, 137–143.

40 M. F. Khan, N. Ahmad, F. K. Alkholifi, Z. Ullah, S. Farooqui, N. Khan, M. S. Khalid, M. N. Ali and H. Tabassum, A Novel UHPLC-MS/MS-Based Bioanalytical Method Developed for S-Allyl Cysteine in the Establishment of a Comparative Pharmacokinetic Study, *Separations*, 2023, **10**, 423, DOI: **10.3390/separations10080423**.

41 H. Bolay and T. Dalkara, Mechanisms of motor dysfunction after transient MCA occlusion: persistent transmission failure in cortical synapses is a major determinant, *Stroke*, 1998, **29**, 1988–1993, DOI: 10.1161/01.STR.29.9.1988; discussion 1994,.

42 K. Fukui, N. O. Omoi, T. Hayasaka, T. Shinnkai, S. Suzuki, K. Abe and S. Urano, Cognitive impairment of rats caused by oxidative stress and aging, and its prevention by vitamin E, *Ann. N. Y. Acad. Sci.*, 2002, **959**, 275–284, DOI: 10.1111/j.1749-6632.2002.tb02099.x.

43 A. J. Hunter, K. B. Mackay and D. C. Rogers, To what extent have functional studies of ischaemia in animals been useful in the assessment of potential neuroprotective agents?, *Trends Pharmacol. Sci.*, 1998, **19**, 59–66, DOI: 10.1016/s0165-6147(97)01157-7.

44 C. Zhan and J. Yang, Protective effects of isoliquiritigenin in transient middle cerebral artery occlusion-induced focal cerebral ischemia in rats, *Pharmacol. Res.*, 2006, **53**, 303–309, DOI: 10.1016/j.phrs.2005.12.008.

45 N. Gull, S. M. Khan, S. Khalid, S. Zia, A. Islam, A. Sabir, M. Sultan, F. Hussain, R. U. Khan and M. T. Z. Butt, Designing of biocompatible and biodegradable chitosan based crosslinked hydrogel for in vitro release of encapsulated povidone-iodine: A clinical translation, *Int. J. Biol. Macromol.*, 2020, **164**, 4370–4380, DOI: 10.1016/j.ijbiomac.2020.09.031.

46 N. Gull, S. M. Khan, O. M. Butt, A. Islam, A. Shah, S. Jabeen, S. U. Khan, A. Khan, R. U. Khan and M. T. Z. Butt, Inflammation targeted chitosan-based hydrogel for controlled release of diclofenac sodium, *Int. J. Biol. Macromol.*, 2020, **162**, 175–187, DOI: 10.1016/j.ijbiomac.2020.06.133.

47 N. Gull, S. M. Khan, M. T. Z. Butt, S. Khalid, M. Shafiq, A. Islam, S. Asim, S. Hafeez and R. U. Khan, In vitro study of chitosan-based multi-responsive hydrogels as drug release vehicles: a preclinical study, *RSC Adv.*, 2019, **9**(53), 31078–31091, DOI: 10.1039/C9RA05025F.

48 N. Gull, S. M. Khan, M. T. Z. Butt, S. Zia, S. Khalid, A. Islam, I. Sajid, R. U. Khan and M. W. King, Hybrid cross-linked hydrogels as a technology platform for in vitro release of cephradine, *Polym. Adv. Technol.*, 2019, **30**(9), 2414–2424, DOI: 10.1002/pat.4688.